Article

The origin of vertebrate teeth and evolution of sensory exoskeletons

https://doi.org/10.1038/s41586-025-08944-w

Received: 4 May 2024

Accepted: 26 March 2025

Published online: 21 May 2025

Open access

Check for updates

Yara Haridy[1]✉, Sam C. P. Norris[1], Matteo Fabbri[1,2], Karma Nanglu[3,4,5], Neelima Sharma[1], James F. Miller[6], Mark Rivers[7], Patrick La Riviere[8], Phillip Vargas[8], Javier Ortega-Hernández[3] & Neil H. Shubin[1]✉

The earliest record of tooth antecedents and the tissue dentine[1,2], an early-vertebrate novelty, has been controversially represented by fragmentary Cambrian fossils identified as *Anatolepis heintzi*[3–5]. *Anatolepis* exoskeletons have the characteristic tubules of dentine that prompted their interpretation as the first precursors of teeth[3], known as odontodes. Debates over whether *Anatolepis* is a legitimate vertebrate[6–8] have arisen because of limitations in imaging and the lack of comparative exoskeletal tissues. Here, to resolve this controversy and understand the origin of dental tissues, we synchrotron-scanned diverse extinct and extant vertebrate and invertebrate exoskeletons. We find that the tubules of *Anatolepis* have been misidentified as dentine tubules and instead represent aglaspidid arthropod sensory sensilla structures[9,10]. Synchrotron scanning reveals that deep ultrastructural similarities between odontodes and sensory structures also extend to definitive vertebrate tissues. External odontodes of the Ordovician vertebrate *Eriptychius*[11–13] feature large dentine tubules[1] that are morphologically convergent with invertebrate sensilla. Immunofluorescence analysis shows that the external odontodes of extant chondrichthyans and teleosts retain extensive innervation suggestive of a sensory function akin to teeth[14–16]. These patterns of convergence and innervation reveal that dentine evolved as a sensory tissue in the exoskeleton of early vertebrates, a function retained in modern vertebrate teeth[16]. Middle-Ordovician fossils now represent the oldest known evidence for vertebrate dental tissues.

The origin of vertebrate teeth has been a long-standing problem in palaeontology[17–24]. Although teeth evolved from structures in the dermal exoskeleton of jawless vertebrates known as odontodes[25], their origin and function remains obscure. Odontodes are the direct evolutionary and developmental antecedents of diverse tooth-like structures, including mandibular and pharyngeal teeth, dermal scales and body denticles[19,25–27]. The odontode unit is characteristically made of dentine, a neural crest-derived vertebrate novelty[2,26,28,29], which has diagnostic internal tubules made by odontoblast processes as they deposit tissue[30]. The presence of dentine in the exoskeleton of Palaeozoic stem-gnathostomes suggests that external odontodes were secondarily recruited into the oral epithelium to form teeth[7–9]. Although dentine seems to be a vertebrate apomorphy, its origins remain controversial owing to its variability, lack of a sufficient comparative dataset, and challenges identifying it in fossil forms.

Cambrian conodonts are the earliest mineralizing vertebrates[31], but remain problematic owing to their uncertain phylogenetic position[17,32–34] and the uniqueness of the mineralized tissues in their pharyngeal elements. Critically, conodont elements lack true dentine[17,34]. The earliest putative occurrence of dentine and odontodes can be traced to fragmentary phosphatic fossils from late-Cambrian and Early-Ordovician deposits known as *Anatolepis heintzi*[3–5]. *Anatolepis* was first described as the earliest agnathan fish[4], but its vertebrate affinity was challenged and instead suggested to correspond to an arthropod exoskeleton on the basis of morphological and histological grounds[6–8]. Researchers then revealed histological details of odontode-specific tissues in *Anatolepis*, such as tubular dentine, a pulp cavity and lamellar basal tissue, which reasserted its position as the first fish[3]. The conclusion that *Anatolepis* represents the earliest mineralizing stem-gnathostome has profound bearing on the initial evolution of vertebrate mineralization, and particularly on the evolution of teeth. If *Anatolepis* embodies the earliest odontodes this would mean dentine and acellular bone were the first vertebrate tissues and enameloid and enamel evolved at a later stage[3,35,36].

The ambiguity of the first vertebrate dental tissues, combined with the lack of comparative data from diverse taxa, restricts our ability to differentiate between several hypotheses on odontode origins including: protection—the dermal skeleton including odontodes evolved as a means against abrasion and predation[25,37,38]; locomotion—increased mineralization in the dermal skeleton acted to stiffen the body in the

[1]Department of Organismal Biology and Anatomy, The University of Chicago, Chicago, IL, USA. [2]Center for Functional Anatomy and Evolution, Johns Hopkins University School of Medicine, Baltimore, MD, USA. [3]Museum of Comparative Zoology, Department of Organismic and Evolutionary Biology, Harvard University, Cambridge, MA, USA. [4]Department of Ecology and Evolutionary Biology, University of Toronto, Toronto, Ontario, Canada. [5]Department of Earth Sciences, University of California, Riverside, Riverside, CA, USA. [6]School of Earth, Environment, and Sustainability, Missouri State University, Springfield, MO, USA. [7]Center for Advanced Radiation Sources, The University of Chicago, Chicago, IL, USA. [8]Department of Radiology, University of Chicago, Chicago, IL, USA. ✉e-mail: Yarah@uchicago.edu; nshubin@uchicago.edu

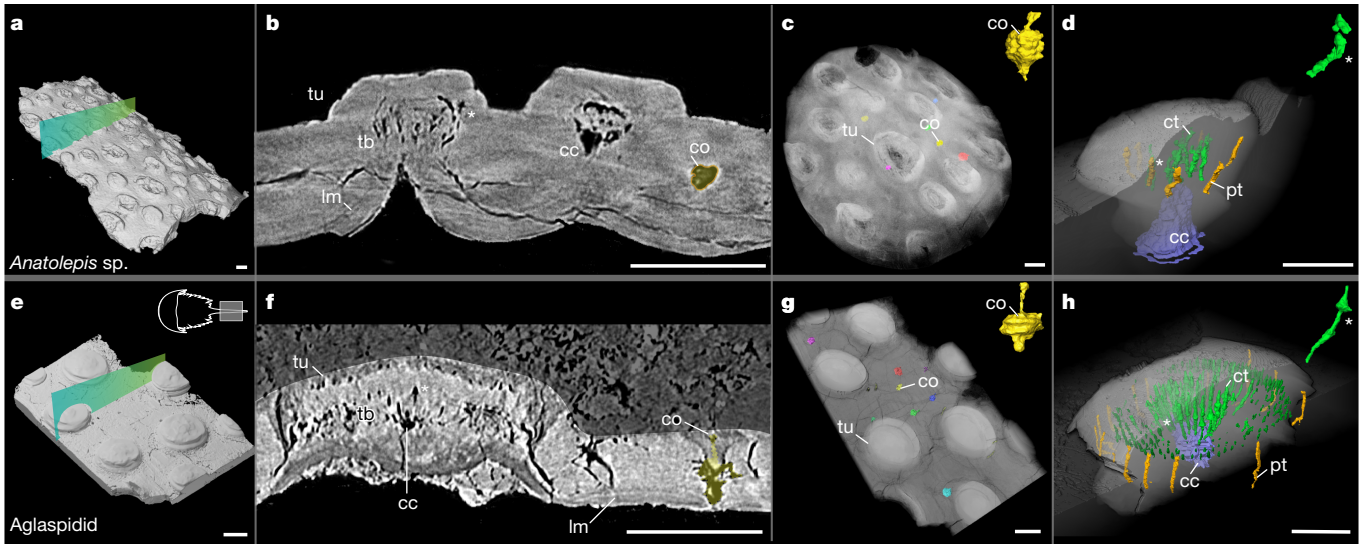

Fig. 1 | Comparative microanatomy of *Anatolepis* sp. and an indeterminate aglaspidid arthropod from the late Cambrian. a, Three-dimensional reconstruction of the late-Cambrian *Anatolepis* sp. fragment from the central Texas Wilberns Formation (TC-1021) with the slice indicating the location of **b**. **b**, Tomographic cross-section of *Anatolepis*. **c**, Translucent three-dimensional reconstruction of the *Anatolepis* fragment with a distribution of segmented cuticle organs in yellow. **d**, Segmented single tubercle of *Anatolepis*. **e**, Three-dimensional reconstruction of an indeterminate aglaspidid tail spine fragment taken from the complete specimen (Milwaukee Public Museum (MPM) 18572), from the late-Cambrian Saint Lawrence Formation of Wisconsin with the slice indicating the location of **f**. **f**, An artificially shaded tomographic cross-section of indeterminate aglaspidid gives contrast to the microanatomy of the tubricle. **g**, Translucent three-dimensional reconstruction of the cuticle of an indeterminate aglaspidid highlighting the distribution of segmented cuticular organs. **h**, Segmented single tubercle of an indeterminate aglaspidid with the central cavity in purple, peripheral tubules in orange, and central tubules in green. cc, central cavity; co, cuticular organ; ct, central tubules; lm, lamellar tissue; pt, peripheral tubule system; tb, tubules; tu, tubercle. The asterisk indicates arrow-shaped tubules in cross-section. Scale bars, 100 µm.

absence of the mineralized axial skeleton[25,39]; mineral storage—the mineralized skeleton evolved for calcium or phosphate storage[25,40]; and sensory—the dermal skeleton evolved as part of, or as a support for, sensory systems[16,25].

In this study we use high-resolution synchrotron computed microtomography to analyse a diverse representation of extant and extinct vertebrate and invertebrate exoskeletons to analyse the origin and distribution of dentine in Cambrian and Ordovician taxa. Together with tissue clearing and immunofluorescence analyses of the external odontodes of extant chondrichthyans and teleosts, our findings illuminate the deep evolutionary origins of dentine and the likely function of the earliest odontodes.

To test the vertebrate affinity of *Anatolepis*, we first deployed high-resolution synchrotron tomography on late-Cambrian fossil fragments. Vertical and horizontal canals infiltrate the mineralized tissue (Fig. 1 and Extended Data Fig. 1) and are connected to teardrop-shaped cavities within an otherwise homogeneous lamellar basal layer (Fig. 1 and Extended Data Fig. 1). The tubercles connect to a central cavity that extends to the ventral surface and dorsally attenuates into multiple large-calibre tubules (Fig. 1h). These features were previously interpreted as a pulp cavity and dentine tubules, respectively, in scanning electron micrographs[3]. Although *Anatolepis'* tubules were difficult to segment because of partial collapse due to acid preparation, tubules can be seen to have a distinct flared arrow-shaped end in the virtual transverse section (Fig. 1b). Tubules are mostly restricted to the centre with a few peripheral tubules that surround the edges of the tubercle (Fig. 1d). Notably, the peripheral tubules had been observed previously in scanning electron micrographs[3] but interpreted as the natural odontode edge. Externally, *Anatolepis* fragments are marked by rounded tubercles that are interspersed and non-overlapping (Fig. 1a and Extended Data Figs. 1 and 2). *Anatolepis'* tubercles vary subtly in morphology and are situated within the thin basal tissue; the tubercles also extend above the basal tissue that is marked externally by several pore openings (Fig. 1 and Extended Data Figs. 1 and 2). The ventral side is covered with dimples that correspond to the location of the tubercles on the opposing side (Fig. 1b). We used this distinct internal and external morphology to match our samples with previously described specimens of *Anatolepis*[3,5].

High-resolution phase-contrast synchrotron scans of coeval aglaspidid arthropod cuticles—extracted from complete specimens—were compared to *Anatolepis*. Similarly to vertebrate skeletons, the exoskeleton of aglaspidids is also phosphatic[41–43]. Aglaspidid cuticles have a homogeneous lamellar structure that is interrupted by vertical pore canals like those described in *Anatolepis*[3] (Fig. 1 and Extended Data Figs. 1–3). Some of these pore canals flare internally into teardrop-shaped cuticular organs, which vary in size through the specimen and are similar to the *Anatolepis* specimens (Fig. 1c,d and Extended Data Figs. 1e,f and 2h). In *Aglaspis? franconensis*, we resolve horizontal canals in addition to the vertical canals and teardrop-shaped cuticular organs. However, this feature was not seen in all scanned aglaspidid cuticle samples and is notably absent from thicker cuticular regions such as portions of the tail spine (Extended Data Fig. 3a,d). Virtual sections indicate partially infilled central cavities from which tubules emanate similar to the putative 'pulp cavities' in *Anatolepis*. The central tubules flare dorsally with a distinctive arrow-shaped cavity, as seen in *Anatolepis*, and are capped by a mineralized cone that sits within a pore (Fig. 2g). Each central tubule is surrounded by a hypermineralized layer that is then surrounded by a hollow cavity, in a tube-in-tube formation that is not seen in vertebrate dentine (Fig. 2e,f). The tubules circumferentially diffuse from the central cavity, and the hollow cavities merge and form a honeycomb structure that is hollow (Fig. 2c,e). Additionally, there is a set of tubules that are peripheral to the central tubules; these are simpler in morphology, lacking both the flared end and mineralized coating (Figs. 1h and 2e). Externally, aglaspidid cuticles have diverse tubercles that vary in size and morphology but are generally rounded, with a corresponding dimple on the underside, the same characters that define *Anatolepis* (Fig. 1a,e). The external morphology, scans and subsequent segmentation of several

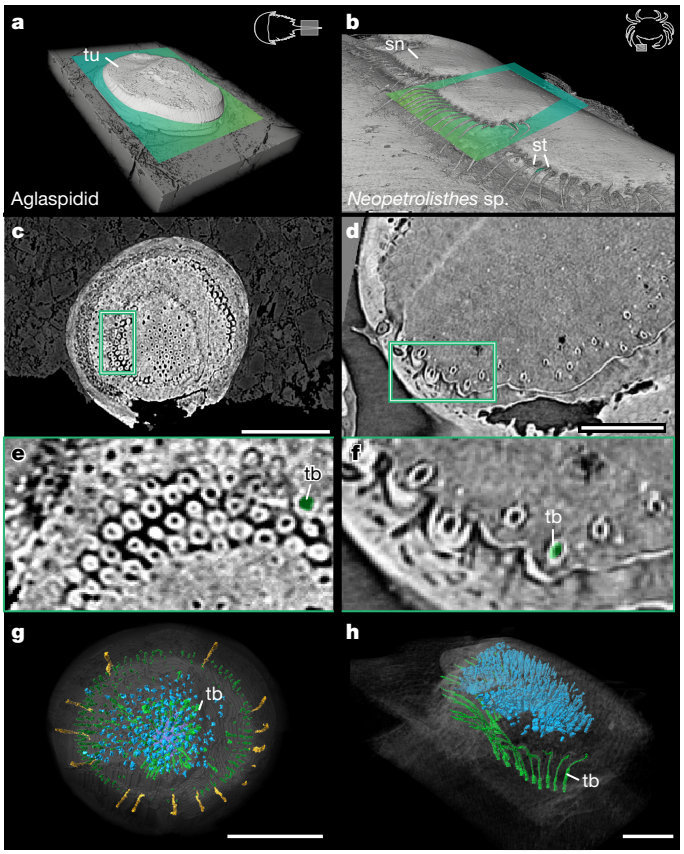

Fig. 2 | Comparison of a late-Cambrian aglaspidid tubercle with extant arthropod sensory sensillum using high-resolution synchrotron tomography. a, Three-dimensional reconstruction of a single tubercle from the tail spine of an indeterminate late-Cambrian aglaspidid from the Saint Lawrence Formation of Wisconsin (MPM 18572) showing a dorsal cross-section indicating the relative region of **c**. **b**, Three-dimensional reconstruction of the claw sensilla of the extant anomuran *Neopetrolisthes* sp. showing the multiple tubercles with emanating setae and a dorsal cross-section indicating the relative region in **d**. **c**, Tomographic dorsal cross-section of indeterminate late-Cambrian aglaspidid (MPM 18572) tubercle. **d**, Tomographic dorsal cross-section of a single sensillum. **e**, A close-up of the dorsally oriented tubules within the tubercle that are composed of a hollow space with a mineralized sheath surrounding a hollow tubule. **f**, A close-up of the extant *Neopetrolisthes* sp. dorsolaterally oriented tubules, exhibiting a hollow tube with a mineralized sheath set into a hollow space. **g**,**h**, Three-dimensional reconstruction showing the internal tubule anatomy of the segmented tubercle and segmented sensilla of the extinct indeterminate aglaspidid (**g**) and extant *Neopetrolisthes* sp. (**h**). In the segmentation images, the tubules showing the tube-in-tube morphology (in green), the peripheral tubules (in yellow) and the top pore spaces (in blue) are highlighted. sn, sensilla; st, seta. Scale bars, 100 μm.

aglaspidid cuticle fragments revealed microanatomy with all of the hallmarks of *Anatolepis*, in having a lamellar basal tissue perforated by vertical and horizontal canals, a central cavity, teardrop-shaped cuticular organs and characteristic arrow-shaped tubules. We conclude that *Anatolepis* is not a vertebrate but is most parsimoniously identified as an aglaspidid arthropod. As this taxon was the only putative stem-gnathostome with dentine from the Cambrian, this identification pushes the earliest definitive occurrence of the clade 40 million years into the Middle Ordovician[6].

To interrogate whether the histological similarities that led to the misidentification of *Anatolepis* reflect deeper similarities between invertebrate and vertebrate exoskeletons, we scanned extant invertebrate cuticle and vertebrate mineralized tissues of 35 extant and extinct genera (Extended Data Table 1). We found that the histology of aglaspidid and *Anatolepis* cuticles did not conform to any dental or osteological tissues seen in the sampled vertebrates but instead was most similar to those of sampled modern arthropod tissues. Specifically, the gnathobases of *Limulus polyphemus* (Atlantic horseshoe crab; Extended Data Fig. 4), the chelicerae of *Hadrurus arizonensis* (giant hairy scorpion; Extended Data Fig. 4), the dactyl sensilla of *Planes mitutus* (Columbus crab; Extended Data Fig. 4) and the dactyl sensilla of *Petrolisthe galathinus* (porcelain crab) have distinct similarities to aglaspidid and *Anatolepis* cuticles (Fig. 2). Owing to the size of the sensilla of the porcelain crab, this specimen resulted in the highest-resolution scan and the best comparison to aglaspidid internal anatomy. Porcelain crab sensilla have the distinctive tube-in-tube morphology of their tubules that emanate from a central cavity and radiate dorsolaterally, terminating in setae (Fig. 2e,f). Overall, the histological microanatomy of the porcelain crab sensilla is most like that of aglaspidid and *Anatolepis* tubercles, with the main difference being a laterally versus circumferentially radiating arrangement of tubules, respectively. The claws and much of the body are covered with sensilla, which are rounded tubercules with seta stemming from one side. Each mineralized seta corresponds to a tube-in-tube structure internally and coalesces past the exocuticle (Fig. 2). In the porcelain crab, the tubercle with setae probably represents a tricoid sensillum[9,10], which is an innervated mechanosensitive receptor sensitive to deflection[10]. The strong similarity between cuticular structures of aglaspidids (including the fragments ascribed to *Anatolepis*) and the sensilla of extant invertebrates suggests that they had a sensory function.

We next examined definitive samples of Middle-Ordovician vertebrate dentine and odontodes to compare them to these invertebrate structures. The microanatomy of the Middle-Ordovician vertebrates is reminiscent of, but distinct from, the invertebrate cuticular tissues described above. Vertebrates from the Middle Ordovician remain largely enigmatic owing to the paucity of specimens. The two most studied taxa are the co-occurring stem-gnathostomes *Eriptychius* and *Astraspis*, which are almost exclusively represented by their odontodes, with rare articulated material confirming stem-gnathostome affinity[1,11,13,44,45]. *Eriptychius* odontodes have a distinct elongate morphology, are made up entirely of dentine and lack a capping enameloid tissue (Fig. 3a,b). Remarkably similar to aglaspidids, *Eriptychius* odontodes have large dentine tubules stemming from a pulp cavity that repeatedly branch and attenuate to the surface as pores as seen also in another Ordovician vertebrate from the Harding sandstone[46,47]. This convergent exposure of tubules to the surface in aglaspidids and *Eriptychius* is suggestive of a sensory function, as is the fact that dentine exposure is the most common cause of painful tooth sensitivity in modern taxa[2]. Additionally, *Eriptychius* odontodes maintain an open pulp cavity that is continuous with the vascular network (Fig. 3c). This is a critical feature when considering the role of vasculature and nerves in the development and maintenance of the pulp cavity, and sensory function[48].

To explore the extent to which the ancestral sensory function of odontodes persists in extant forms, we tested for innervation in the external odontodes from a diverse range of extant fishes. Dental innervation studies are typically based on oral teeth[48–50] rather than external odontodes, limiting our inferences on the original function of these structures. Given that external odontodes are homologous to teeth, innervation probably also has a crucial role in the development and function of odontodes. We tested this hypothesis through tissue clearing and immunofluorescence analysis on tail odontodes from late developmental stages and juvenile catsharks (*Scyliorhinus retifer*; Fig. 4) and little skates (*Leucoraja erinacea*; Extended Data Fig. 5), and the pectoral fin odontodes of juvenile bristlenose catfish (*Ancistrus* sp.; Fig. 4). Three-dimensional segmentation of confocal stacks shows innervation associated with odontodes to be present in all taxa sampled, with nerves surrounding the base of odontodes

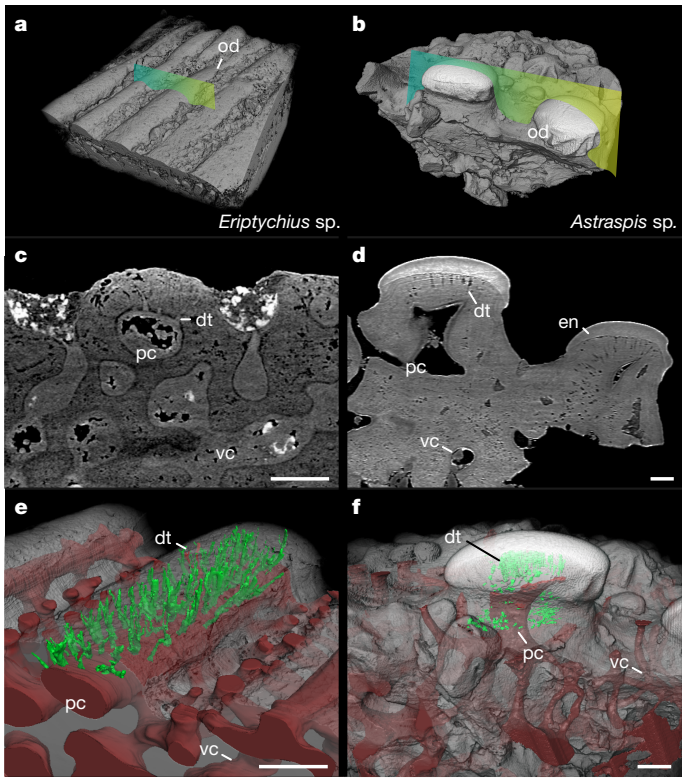

Fig. 3 | Odontode microanatomy in the Middle-Ordovician agnathan vertebrates *Eriptychius* and *Astraspis*. **a**, Three-dimensional reconstruction of a fragment of dermal armour of the agnathan *Eriptychius* sp. (Field Museum of Natural History (FMNH) PF 17901) showing the elongated odontodes and a transverse section indicating the relative region of **c**. **b**, Three-dimensional reconstruction of a fragment of dermal armour of the agnathan *Astraspis* sp. (FMNH PF 17898) showing the rounded and stellate-shaped odontodes and a transverse section indicating the relative region of **d**. **c**, A transverse tomographic section of *Eriptychius* sp. odontodes exhibiting a lack of enameloid, wide-calibre dentine tubules, pulp cavity and vascular canals. **d**, A transverse tomographic section of *Astraspis* sp. odontodes exhibiting a thick layer of enameloid, narrow-calibre dentine tubules, pulp cavity and vascular canals. **e**,**f**, Three-dimensional reconstruction showing the internal anatomy of *Eriptychius* sp. and *Astraspis* sp.; note the lack of enamel, wide-calibre dentine tubules and extensive vascularity of *Eriptychius* sp. dt, dentine tubule; en, enameloid; od, odontode; pc, pulp cavity; vc, vascular canal. Scale bars, 100 µm.

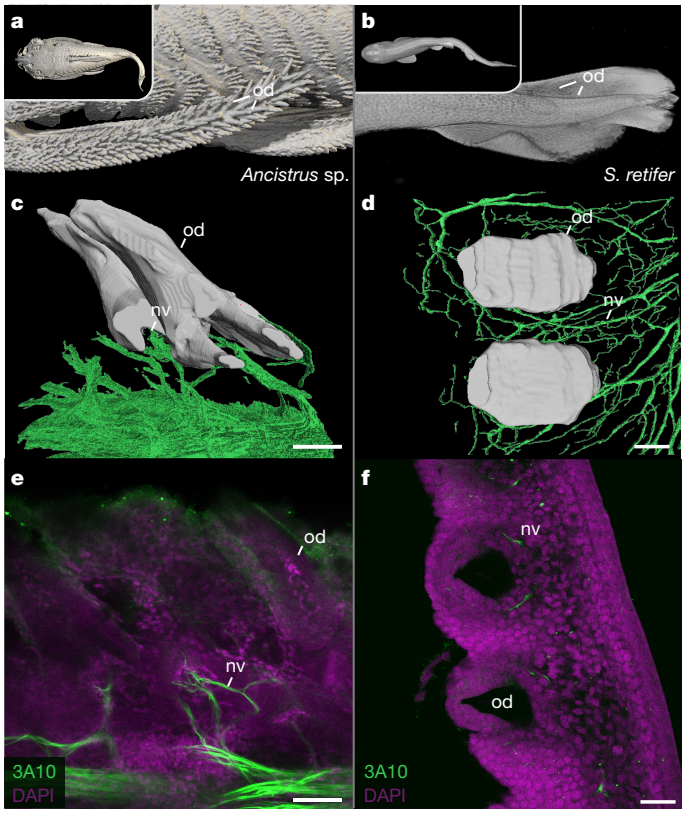

Fig. 4 | Innervation of external odontodes in the extant teleost *Ancistrus* and the extant chondrichthyan *Scyliorhinus*. **a**, Adult bristlenose catfish (*Ancistrus* sp.) showing odontode-covered dermal armour and an odontode-covered fin. **b**, Juvenile catshark (*S. retifer*) showing odontodes along the entire body, with a close-up of the tail region. **c**, *Ancistrus* sp. immunofluorescence confocal stack-based segmentation of fin odontodes with nerves branching and entering the pulp cavity of the odontodes. **d**, Dorsal view of *S. rotifer* immunofluorescence confocal stack-based segmentation of tail odontodes with nerves associated with odontodes. **e**, Immunostained cross-section of *Ancistrus* sp. fin odontodes showing the innervation of the pulp cavity at the base of the odontode with multiple branching nerves. **f**, Dorsal view of immunostained catshark tail tip odontodes, with nerves surrounding and associated with the forming odontode. This experiment was performed on one representative sample of the correct stage in each species, $n = 1$. nv, nerves; 3A10, neurofilament marker; DAPI, 4′,6-diamidino-2-phenylindole, dihydrochloride. Scale bars, 50 µm.

in chondrichthyans and invading the pulp cavity in the pectoral fin in the catfish (Fig. 4). These findings support the hypothesis that the innervation associated with the dentine of odontodes is an ancestral trait among extant gnathostomes.

Discussion

Anatolepis' putative vertebrate affinities hinged on two main arguments, namely the absence of a complex pore canal system in arthropod cuticles, and the presence of dentine, a calcified tissue of neural crest origin unique to vertebrates. Our data show that late-Cambrian *Anatolepis* and aglaspidid arthropods and modern arthropods have a cuticle with a pore canal arrangement (Extended Data Fig. 1), which includes sensilla with tubules radiating from a central cavity (Figs. 1, 2 and 5 and Extended Data Figs. 1, 2, 4 and 6). Our new high-resolution synchrotron scan data demonstrate that the seemingly simple dentine tubules in the tubercles of *Anatolepis* are in reality complex tubules with distinct morphology that more closely conform to arthropod sensilla found in Cambrian aglaspidids and modern arthropods[9,10,51]. Thus, the fossil tissues of *Anatolepis* are not dentine and lamellar bone, as they do not conform to any known variation found in extinct or extant vertebrates, but instead correspond to an arthropod exoskeleton as expressed in both extinct and extant species[52,53].

The removal of *Anatolepis* from vertebrates means that the presence of enamel or enameloid at the origin of odontodes can be tracked to the Middle Ordovician[22,28,45]. The only other putative Cambrian armoured agnathan is an unnamed taxon originating from Australia with the fragmentary material being compared to the Ordovician pteraspidomorph agnathan *Porophoraspis*[54]. However, the described histology of this Cambrian Australian material also reveals more similarities to arthropod cuticle than to any known vertebrate. The horizontal and vertical canals are similar to those we describe in aglaspidids and other arthropods, and granular middle layers with distinct polygons[54] are seen in many arthropods including the porcelain crab (*P. galathinus*) in this study (Extended Data Fig. 6).

The odontodes of early vertebrates such as *Eriptychius* have clear markers of sensory capability, such as an open pulp cavity, large dentine tubules and a lack enameloid. The lack of capping enameloid

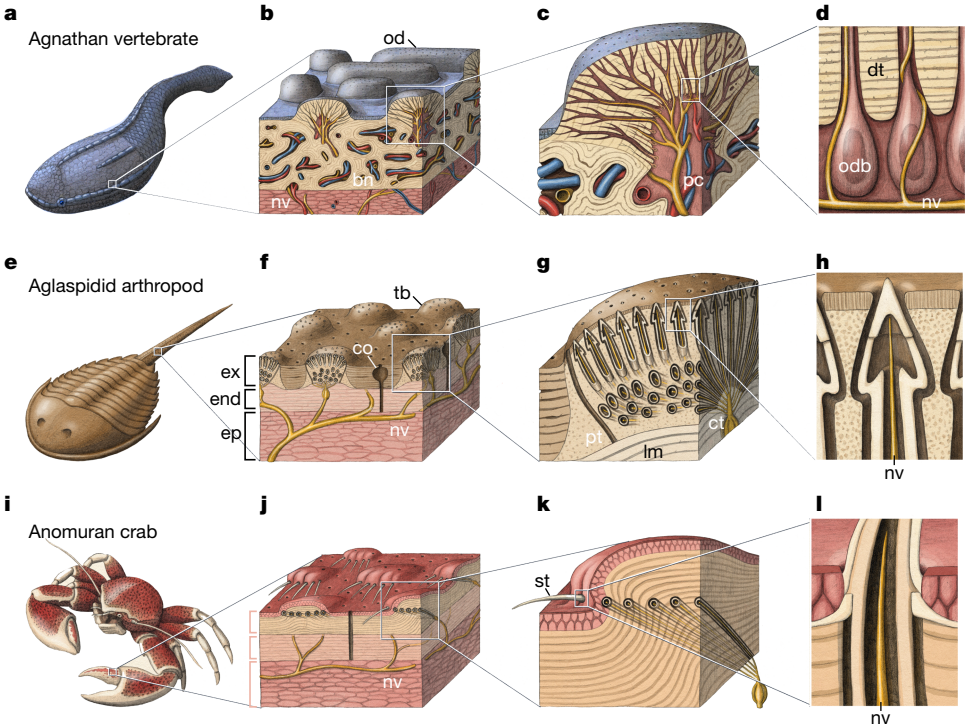

Fig. 5 | Ultrastructural similarities between vertebrate odontodes and arthropod sensorial structures. a, Artistic reconstruction of the Ordovician agnathan *Astraspis* sp. as a representative of an early mineralizing vertebrate. **b**, Schematic illustration of the elongate odontode system in the agnathan *Eriptychius* sp. **c**, Magnification of a single odontode of *Eriptychius* sp. exhibiting the wide-calibre dentine tubules and pulp cavity. **d**, Magnification of the intradental innervation at the pulp–dentine border zone, where innervation potentially extends into the dentine tubules alongside the odontoblasts. **e**, Artistic reconstruction of Cambrian aglaspidid *Aglaspis* sp. **f**, Schematic illustration of the mineralized exoskeleton of an aglaspidid showing cuticle organization and tubercles. **g**, Close-up of a single aglaspidid tubercle showing the radiating arrangement of the tubules, the mineralized coating of the tubules, peripheral tubules and the arrow-shaped termination of the tubules. **h**, Close-up of the termination of the tubules of an aglaspidid near the surface of the tubercle. **i**, An artistic rendering of the extant anomuran *Neopetrolisthes* sp. **j**, Schematic illustration of *Neopetrolisthes* sp. sensilla on the cuticle. **k**, Close-up of a single sensillum with tubules emanating dorsolaterally to the seta. **l**, Close-up of the *Neopetrolisthes* sp. terminal end of a tubule into a single seta. bn, bone; ct, central tubule; end, endocuticle; ep, epidermis; ex, exocuticle; odb, odontoblast. The illustrations were created by A. Boersma under a Creative Commons licence CC BY-SA 4.0.

in *Eriptychius* would have allowed dentine tubules to be exposed to surface stimuli, which in modern taxa causes extreme sensitivity[14,55]. Additionally, the large-calibre dentine tubules in the odontodes of *Eriptychius* indicate the persistent presence of odontoblast processes, which have been shown to act as sensory receptors in teeth[16]. The open pulp cavity of *Eriptychius* odontodes implies innervation, as dental studies indicate critical cross-talk between the dental mesenchyme and the development and maintenance of innervation in open pulp cavity[48] (see the discussion on dental sensitivity in the Supplementary Information). By contrast, co-occurring *Astraspis* odontodes have a thick layer of hypermineralized enameloid, blocking the small-calibre dentine tubuli from being exposed to the surface, and the pulp cavity is gradually infilled in older odontodes, probably leading to a diminished sensory function (Fig. 4). On the basis of these observations, we reason that *Eriptychius* odontodes were more suited to sensory capability than those of *Astraspis*.

Sensory capabilities are crucial to maintaining environmental awareness in an organism covered by external protective armour, whether in vertebrates or invertebrates. This biological demand led to the remarkable convergence of early-vertebrate dermal odontodes and arthropod cuticle sensilla, which along with the lateral lines in vertebrates contribute to 'sensory armour' (Fig. 5). Indeed, arthropod cuticles with pore canal systems are part of advanced and highly specialized sensory organs that have been documented in modern taxa[10,51,52] but largely overlooked in the fossil record.

An ancestral sensory function of dentine reveals that independent vertebrate dental specializations, or autapomorphies, reflect a shared history. Notably, there are numerous reports of modern vertebrates with sensitive external odontodes. Blind catfish have specialized dermal odontodes that have a purported sensory function[56,57]. Several mammals, such as narwhals, have specialized dentition that serves a sensory function[58–60]. Odontoblasts themselves are widely recognized to be sensory cells[14,16,55]. When viewed through this evolutionary lens, the fact that teeth in the mouth are extremely sensitive is less of a mystery, and more a reflection of their evolutionary origins within the sensory armour of early vertebrates.

Online content

Any methods, additional references, Nature Portfolio reporting summaries, source data, extended data, supplementary information, acknowledgements, peer review information; details of author contributions and competing interests; and statements of data and code availability are available at https://doi.org/10.1038/s41586-025-08944-w.

1. Smith, M. M. & Sansom, I. J. in *Development, Function and Evolution of Teeth* (eds Teaford M.F. et al.) Ch. 5 (Cambridge Univ. Press, 2000).
2. Gans, C. & Northcutt, R. G. Neural crest and the origin of vertebrates: a new head. *Science* **220**, 268–273 (1983).
3. Smith, M. P., Sansom, I. J. & Repetski, J. E. Histology of the first fish. *Nature* **380**, 702–704 (1996).
4. Bockelie, T. & Fortey, R. A. An early Ordovician vertebrate. *Nature* **260**, 36–38 (1976).
5. Repetski, J. E. A fish from the Upper Cambrian of North America. *Science* **200**, 529–531 (1978).
6. Paul Smith, M. & Sansom, I. J. The affinity of *Anatolepis* Bockelie & Fortey. *Geobios* **28**, 61–63 (1995).

7. Peel, J. S. & Higgins, A. K. *Anatolepis* - a problematic Ordovician vertebrate reinterpreted as an arthropod. *Rapp. Grønl. Geol. Unders.* **85**, 108–109 (1977).
8. Peel, J. S. *Anatolepis* from the Early Ordovician of East Greenland - not a fishy tail. *Rapp. Grønl. Geol. Unders.* **91**, 111–115 (1979).
9. Naimark, E.B. & Chaika, S.Y. The complex structure of the cuticle of *Pseudagnostus* (Agnostina, Trilobita?). *Paleontol. J.* **57**, 762–774 (2023).
10. Keil, T. A. Comparative morphogenesis of sensilla: a review. *Int. J. Insect Morphol. Embryol.* **26**, 151–160 (1997).
11. Bryant, W. L. A study of the oldest known vertebrates, *Astraspis* and *Eriptychius*. *Proc. Am. Philos. Soc.* **76**, 409–427 (1936).
12. Sansom, I. J., Smith, M. P., Smith, M. M. & Turner, P. The Harding Sandstone revisited -a new look at some old bones. *Geobios* **28**, 57–59 (1995).
13. Dearden, R. P. et al. The oldest three-dimensionally preserved vertebrate neurocranium. *Nature* https://doi.org/10.1038/s41586-023-06538-y (2023).
14. Pashley, D. H. Mechanisms of dentin sensitivity. *Dent. Clin. North Am.* **34**, 449–473 (1990).
15. Byers, M. R. in *International Review of Neurobiology* Vol. 25 (eds Smythies, J. R. & Bradley, R. J.) 39–94 (Elsevier, 1984).
16. Magloire, H., Couble, M.-L., Thivichon-Prince, B., Maurin, J.-C. & Bleicher, F. Odontoblast: a mechano-sensory cell. *J. Exp. Zool. B* **312B**, 416–424 (2009).
17. Murdock, D. J. E. et al. The origin of conodonts and of vertebrate mineralized skeletons. *Nature* **502**, 546–549 (2013).
18. Donoghue, P. C. J. & Rücklin, M. The ins and outs of the evolutionary origin of teeth. *Evol. Dev.* **18**, 19–30 (2016).
19. Fraser, G. J., Cerny, R., Soukup, V., Bronner-Fraser, M. & Streelman, J. T. The odontode explosion: the origin of tooth-like structures in vertebrates. *BioEssays* **32**, 808–817 (2010).
20. Donoghue, P. Evolution: divining the nature of the ancestral vertebrate. *Curr. Biol.* **27**, R277–R279 (2017).
21. Huysseune, A., Sire, J.-Y. & Witten, P. E. Evolutionary and developmental origins of the vertebrate dentition. *J. Anat.* **214**, 465–476 (2009).
22. Donoghue, P. C. J. & Sansom, I. J. Origin and early evolution of vertebrate skeletonization. *Microsc. Res. Tech.* **59**, 352–372 (2002).
23. Rücklin, M. & Donoghue, P.C. in *eLS*, https://doi.org/10.1002/9780470015902.a0026408 (John Wiley & Sons, 2025).
24. Ahlberg, P.E. (ed.) *Major Events in Early Vertebrate Evolution*, 1st edn (CRC Press, 2001).
25. Reif, W.-E. in *Evolutionary Biology* (eds Hecht, M. K. et al.) 287–368 (Springer, 1982).
26. Debiais-Thibaud, M. et al. The homology of odontodes in gnathostomes: insights from Dlx gene expression in the dogfish, *Scyliorhinus canicula*. *BMC Evol. Biol.* **11**, 307 (2011).
27. Haridy, Y., Gee, B. M., Witzmann, F., Bevitt, J. J. & Reisz, R. R. Retention of fish-like odontode overgrowth in Permian tetrapod dentition supports outside-in theory of tooth origins. *Biol. Lett.* **15**, 20190514 (2019).
28. Smith, M. M. Putative skeletal neural crest cells in early Late Ordovician vertebrates from Colorado. *Science* **251**, 301–303 (1991).
29. Stundl, J. et al. Ancient vertebrate dermal armor evolved from trunk neural crest. *Proc. Natl Acad. Sci. USA* **120**, e2221120120 (2023).
30. Couve, E., Osorio, R. & Schmachtenberg, O. The amazing odontoblast: activity, autophagy, and aging. *J. Dent. Res.* **92**, 765–772 (2013).
31. Sansom, I. J., Smith, M. P., Armstrong, H. A. & Smith, M. M. Presence of the earliest vertebrate hard tissue in conodonts. *Science* **256**, 1308–1311 (1992).
32. Blieck, A. et al. Fossils, histology, and phylogeny: why conodonts are not vertebrates. *Epidodes* **33**, 234–241 (2010).
33. Miyashita, T. et al. Hagfish from the Cretaceous Tethys Sea and a reconciliation of the morphological–molecular conflict in early vertebrate phylogeny. *Proc. Natl Acad. Sci. USA* **116**, 2146–2151 (2019).
34. Turner, S. et al. False teeth: conodont-vertebrate phylogenetic relationships revisited. *Geodiversitas* **32**, 545–594 (2010).
35. Qu, Q., Haitina, T., Zhu, M. & Ahlberg, P. New genomic and fossil data illuminate the origin of enamel. *Nature* **526**, 108–111 (2015).
36. Sire, J.-Y., Davit-Béal, T., Delgado, S. & Gu, X. The origin and evolution of enamel mineralization genes. *Cells Tissues Organs* **186**, 25–48 (2007).
37. Lebedev, O. A., Mark-Kurik, E., Karatajūtė-Talimaa, V. N., Lukševičs, E. & Ivanov, A. Bite marks as evidence of predation in early vertebrates. *Acta Zool.* **90**, 344–356 (2009).
38. Halstead, L. B. *Vertebrate Hard Tissues* (Wykeham, 1974).
39. Wainwright, S. A., Vosburgh, F. & Hebrank, J. H. Shark skin: function in locomotion. *Science* **202**, 747–749 (1978).
40. Haridy, Y. et al. Bone metabolism and evolutionary origin of osteocytes: novel application of FIB-SEM tomography. *Sci. Adv.* **7**, eabb9113 (2021).
41. Hesselbo, S. P. Aglaspidida (Arthropoda) from the Upper Cambrian of Wisconsin. *J. Paleontol.* **66**, 885–923 (1992).
42. Briggs, D. E. G. & Fortey, R. A. The cuticle of the aglaspidid arthropods, a red-herring in the early history of the vertebrates. *Lethaia* **15**, 25–29 (1982).
43. Lerosey-Aubril, R., Ortega-Hernández, J., Kier, C. & Bonino, E. Occurrence of the Ordovician-type aglaspidid *Tremaglaspis* in the Cambrian Weeks Formation (Utah, USA). *Geol. Mag.* **150**, 945–951 (2013).
44. Sansom, I. J., Smith, M. P., Smith, M. M. & Turner, P. *Astraspis*-the anatomy and histology of an Ordovician fish. *Palaeontology* **40**, 625–643 (1997).
45. Denison, R. H. *Ordovician Vertebrates from Western United States* (Field Museum of Natural History, 1967).
46. Sansom, I. J., Smith, M. M. & Smith, M. P. Scales of thelodont and shark-like fishes from the Ordovician of Colorado. *Nature* **379**, 628–630 (1996).
47. Johanson, Z., Tanaka, M., Harriman, N. & Meredith Smith, M. Early Palaeozoic dentine and patterned scales in the embryonic catshark tail. *Biol. Lett.* **4**, 87–90 (2007).
48. Fried, K. & Gibbs, J. in *The Dental Pulp: Biology, Pathology, and Regenerative Therapies* (ed. Goldberg, S.) 75–95 (Springer, 2014).
49. Kollar, E. J. & Lumsden, A. G. Tooth morphogenesis: the role of the innervation during induction and pattern formation. *J. Biol. Buccale* **7**, 49–60 (1979).
50. Lumsden, A. G. S. & Buchanan, J. A. G. An experimental study of timing and topography of early tooth development in the mouse embryo with an analysis of the role of innervation. *Arch. Oral Biol.* **31**, 301–311 (1986).
51. Albert, P. J., Zacharuk, R. Y. & Wong, L. Structure, innervation, and distribution of sensilla on the wings of a grasshopper. *Can. J. Zool.* **54**, 1542–1553 (1976).
52. Locke, M. Pore canals and related structures in insect cuticle. *J. Biophys. Biochem. Cytol.* **10**, 589–618 (1961).
53. Wigglesworth, V. B. The transfer of lipid in insects from the epidermal cells to the cuticle. *Tissue Cell* **17**, 249–265 (1985).
54. Young, G. C., Karatajute-Talimaa, V. N. & Smith, M. M. A possible Late Cambrian vertebrate from Australia. *Nature* **383**, 810–812 (1996).
55. Kim, J. W. & Park, J.-C. Dentin hypersensitivity and emerging concepts for treatments. *J. Oral Biosci.* **59**, 211–217 (2017).
56. Haspel, G., Schwartz, A., Streets, A., Camacho, D. E. & Soares, D. By the teeth of their skin, cavefish find their way. *Curr. Biol.* **22**, R629–R630 (2012).
57. Schaefer, S. A. & Buitrago-Suárez, U. A. Odontode morphology and skin surface features of Andean astroblepid catfishes (Siluriformes, Astroblepidae): Odontode morphology. *J. Morphol.* **254**, 139–148 (2002).
58. Nweeia, M. T. et al. Sensory ability in the narwhal tooth organ system. *Anat. Rec.* **297**, 599–617 (2014).
59. Catania, K. C. & Remple, M. S. Somatosensory cortex dominated by the representation of teeth in the naked mole-rat brain. *Proc. Natl Acad. Sci. USA* **99**, 5692–5697 (2002).
60. Weissengruber, G. E., Egerbacher, M. & Forstenpointner, G. Structure and innervation of the tusk pulp in the African elephant (*Loxodonta africana*). *J. Anat.* **206**, 387–393 (2005).

Methods

Fossil specimens

***Anatolepis*.** The original described material[3–5] was not available or could not be located owing to collections moving from Denver to the Smithsonian National Museum of Natural History (USNM) and other non-returned loans. The *Anatolepis* material in this study is from Miller's sample TC-1021, from central Texas and from near the top of the Morgan Creek Limestone Member of the Wilberns Formation[61]. Limestone at that stratigraphic horizon is assigned to the trilobite *Idahoia* Zone. The strata are from the Sunwaptan Stage of the Millardan Series, late Cambrian in age[61]. At the time of collection, a 2–3-kg limestone sample was dissolved in ≈15% glacial acetic acid. The dissolved material was wet-sieved, and the insoluble residue was dried. This residue was concentrated using a dense liquid, 1,1,2,2 tetrabromoethane, with a specific gravity of about 2.87. Conodonts, fragments of *Anatolepis* and other phosphatic fossils were concentrated in the dense fraction. The fossils were picked from the dense fraction with a fine artist's paintbrush under ×25 magnification with a binocular microscope. Additional '*Anatolepis*' was provided by the Geological Survey of Canada (GSC), for external examination and scanning but no destructive sampling was permitted. The following '*Anatolepis*' specimens were examined: GSC 65600, GSC 65601 and GSC 65602. Additionally, two specimens of 'undetermined fish A' (GSC 65598 and GSC 65599) and two specimens of 'undetermined fish B' (GSC 65603 and GSC 65604) were examined. All GSC specimens are from the Cow Head Group, a deposition at the eastern edge of the North American continent spanning an interval extending from the middle Cambrian to the base of the Middle Ordovician, and have been previously published[62]. All Cow Head specimens appeared to correspond to arthropod invertebrate cuticle.

Aglaspidid. MPM 18572 is a telson fragment removed from a mostly complete articulated individual, and is featured in Figs. 1 and 2. However, we examined and scanned many more aglaspidids. All examined late-Cambrian aglaspidid material was from the Raasch[63] collection, which is split between the USNM, Washington, DC and the MPM, Milwaukee, with some material collected by G. Gunderson and donated to the University of Wisconsin Geology Museum. All of the late-Cambrian aglaspidids sampled here come from the Upper Cambrian of the Saint Lawrence Formation, Sauk County, WI (see ref. 63 for other locality details).

***Aglaspis? franconensis*.** The *Aglaspis? franconensis* holotype USNM PAL 98916, from the '*Ptychaspis* beds' of the Tunnel City Group at Hudson, Saint Croix County, WI[41] (see ref. 63 for other locality details), was sampled. Permission for destructive sampling of the *Aglaspis? franconensis* USNM PAL 98916 holotype was obtained from the USNM, granted by C. Labanderia, to sample a small fragment of the exoskeleton for comparative purposes. The fragment was then mounted with reversible glue on a plastic toothpick and labelled for synchrotron scanning.

***Astraspis* sp.** FMNH PF 17898 is a fragment of dermal bone with several odontodes ankylosed. This was picked from loose dissolved material, and then mounted on a plastic toothpick with reversible glue for scanning. The stellate and round morphology identifies the fragment as *Astraspis* sp.[11,44,64]. This specimen originates from the Middle-Ordovician Harding Sandstone of Wyoming[11,12].

***Eriptychius* sp.** FMNH PF 17901 is a fragment of dermal bone with several elongate odontodes ankylosed. This was picked from loose dissolved material, and then mounted on a plastic toothpick with reversible glue for scanning. The elongate odontode morphology and lack of dentine identify the fragment as *Eryptychius* sp.[11,65]. This specimen originates from the Middle-Ordovician Harding Sandstone of Wyoming[11,12].

Extant specimens

Invertebrate procurement. Samples of *Polites* sp. and shed exoskeletons of *Petrolisthes galathinus* (porcelain crab) were donated by C. Ferret, from his own collection. *Limulus polyphemus* (Atlantic horseshoe crab), *Callinectes sapidus* (Atlantic blue crab), *Planorbarius corneus* (ramshorn snail), *Eupatorus gracilicornis* (five-horned rhinoceros beetle) and *Megabalanus tintinnabulum* (giant purple barnacle) were purchased online as pinned or desiccated specimens. All other extant invertebrate cuticles came from the FMNH ethanol collections and were not from animals killed for this project (see Extended Data Table 1).

Vertebrate procurement, care and procedures. Suckermouth armoured catfish (*Ancistrus* sp.) were purchased from a local aquarium store (NationWideAquaticsUSA) and were bred in aquarium tanks following a slightly modified version of the protocol described in ref. 66. In this study, we used the albino and 'lemon' morphs for their reduced melanin; however, these lines have potentially been hybridized in the hobby, and therefore an exact species is uncertain. Water was replaced once a week with dechlorinated water prepared from tap water using chlorine remover treatment (API, tap water conditioner). Water changes with cold water were increased when breeding behaviour was observed. The water was maintained at 27 °C and pH 6.5–7. The temperature was reduced by up to 3 °C by unplugging the heater and doing cold water changes to simulate the rainy season until eggs were laid. Each tank contained one male and two to three female fish, allowing natural breeding. Ceramic D-shaped caves were placed in the tanks to allow for the males to establish territories and the females to lay eggs in them. Once eggs were laid, they were removed from the cave and placed in a jar with a bubbler. Juveniles and adult fish were fed boiled vegetables and algae wafers. Guidelines for animal rearing were approved by The Institutional Animal Care and Use Committees (IACUC) of the University of Chicago who approved the care and breeding of *Ancistrus* sp. (bristlenose catfish) (IACUC number 72734). All of the procedures were performed at the University of Chicago.

The hatchling *Leucoraja erinacea* (little skate) and hatchling *Scyliorhinus retifer* (catsharks) were obtained from the Marine Resources Center, Marine Biological Laboratory, Woods Hole, MA, USA. All animals were euthanized using 0.5% tricaine methanesulfonate (MS-222, Syndel) until the cessation of heartbeat and fixed in 4% paraformaldehyde (PFA; Acros Organics, item number EW-88353-82) overnight before transferring them to 1× phosphate-buffered saline (PBS; Fisher Bioreagents).

Acquisition of the synchrotron micro-computed tomography dataset

Synchrotron micro-computed tomography was performed at beamline 13-BM-D at the Advanced Photon Source at Argonne National Laboratory. The white X-ray beam from the Advanced Photon Source bending magnet was reflected from a Pt-coated mirror at a 3 mrad incidence angle, producing an energy spectrum centred at about 25 keV with approximately 10 keV bandwidth. A total of 3,600 projection views were acquired over 180° using a Point Grey Grasshopper 3 camera, with 1,920 (horizontal) × 1,200 (vertical) pixels, and a LuAG scintillator. The sample-to-scintillator distance was approximately 45 mm. Depending on the sample, the camera was equipped with either a 10× or 5× Mitutoyo long-working-distance objective lens. For both objectives, a 175-mm tube was used, resulting in 0.56-μm pixels in object space for the 10× lens and 1.09-μm pixels in object space for the 5× lens. The exposure time was 0.014 s per view for the 10× lens and 0.025 s per view for the 5× lens. Images were reconstructed using the GSECARS tomography processing software (https://cars-uchicago.github.io/IDL_Tomography/)[67], which dark-current-corrects and white-field-normalizes the acquired data before performing gridding-based image reconstruction. The resulting image voxel sizes are 0.56 × 0.56 × 0.56 μm for the 10×

configuration and 1.09 × 1.09 × 1.09 µm for the 5× configuration. The experiment was run at GSECARS; proposal GUP: 82458; proposal title: Characterizing the origin and development of the earliest mineralizing tissues in vertebrates using synchrotron micro-computed tomography; experiment dates: 21 March 2023 and 2 December 2022.

Acquisition of the laboratory micro-computed tomography dataset

Laboratory micro-computed tomography was performed on a Phoenix v|tome|x S 240 from GE (PaleoCT facility, RRID: SCR024763, University of Chicago) using the 180-kV nano-focus tube. The scanning parameters for *S. retifer* (stage 38 catshark) were 70-kV tube voltage and 400-µA tube current, with a timing of 100 ms, 2,000 projections, 3-frame averaging and a 0.1 Cu filter applied; the voxel size was 10.256 µm. For *L. erinacea* (stage 33 little skate), the parameters were 100 kV and 135 µA, with a timing of 150 ms, 3-frame averaging, resulting in a voxel size of 26.181. For the *Ancistrus* sp. (bristlenose catfish), the parameters were 60 kV and 269 µA tube current, with a timing of 100 ms, 2,000 projections and 3-frame averaging; the voxel size was 35.062. Segmentation, reconstruction and visualization were performed on Amira 3D 2021.1 (Konrad-Zuse-Zentrum Berlin, 1995–2001 and FEI SAS, a part of Thermo Fisher Scientific, 1999–2021).

Collection of embryos and fixation

Fertilized eggs of *S. retifer* and *L. erinacea* were obtained from the Marine Biological Laboratory facilities (https://www.mbl.edu/research/research-organisms). Embryos of *S. retifer* (stage 38, following ref. 68) and *L. erinacea* (stages 31 and 32 ($n = 4$), following ref. 69, in addition to 2-week-old hatchlings ($n = 6$)) were mechanically extracted and placed in 0.5% tricaine diluted in 1% PBS for 30 min. Embryos were then fixed in freshly made 4% PFA in PBS for 4 days on a rocker at 4 °C. The samples were then dehydrated in 25%, 50%, 75% and then 100% methanol and stored at −20 °C.

Tissue clearing and immunofluorescence labelling

To acquire whole-odontode images of immunofluorescently labelled tissue with a confocal microscope, samples were optically cleared using modified versions of previously established techniques[70–73].

Juvenile bristlenose catfish (*Ancistrus* sp.) were first rehydrated (100%, 75%, 50%, 25% and 0% methanol in 1× PBS). The rehydrated samples were then delipidated in a solution of 10 w/v% Triton X-100 (Fisher Scientific, BP151) and 10 w/v% *N*-butyldiethanolamine (Alfa Aesar, L09953.22) dissolved in distilled water (CUBIC-L)[70] for 5 days, gently shaking at 37 °C, with the CUBIC-L solution changed daily. The samples were then washed in 1× PBS six times for 2 h each, with one wash left overnight. Samples were then blocked overnight at 4 °C while shaking in blocking buffer (5 v/v% goat serum (Gibco, 16210-072, lot 2285796), 1 w/v% bovine serum albumin (Fisher Scientific, BP9704, lot 222347) and 0.3 v/v% Triton X-100 in 1 × PBS) before immunostaining. The next day, samples were incubated in primary antibodies to neurofilament-associated antigens (Developmental Studies Hybridoma Bank, clone 3A10, lot 5/7/20; 1:100 in blocking buffer) for 7 days at 4 °C while shaking. Samples were then washed in blocking buffer three times for 2 h each, with one wash left overnight. Samples were then stained with secondary antibodies (Cy3 donkey anti-mouse IgG, Jackson Laboratories, 715-165-150, lot 163873; 1:300) and counterstained with DAPI (Biotium, 40009, lot 15D1117; 1:1,000) in blocking buffer for 7 days at 4 °C while shaking. Samples were then washed in 1 × PBS three times for 2 h each and postfixed overnight in 1 w/v% PFA in 1× PBS overnight at 4 °C while shaking. Samples were washed with 1 × PBS for 2 h before preparing them for confocal microscopy.

We found that embryonic *S. retifer* and *L. erinacea* tissues were more difficult to image, probably owing to larger tissue sizes and increased extracellular matrix protein concentration; thus, additional steps were required to optically clear the tissue samples. Samples were first bleached to reduce autofluorescence and pigmentation into a solution of methanol, dimethylsulfoxide and 30% hydrogen peroxide (4:1:1) while exposed under constant light overnight. After this, samples were rehydrated (100%, 75%, 50%, 25% and 0% methanol in PBS 1%). The rehydrated samples were then delipidated in CUBIC-L as described above. To increase antibody penetration and optical transparency, samples were enzymatically digested with collagenase P. Samples were first immersed in reaction buffer for 2 h at 37 °C while shaking, and then digested in a solution of 1 mg ml^{-1} collagenase P in carbonate buffer (50 mM sodium carbonate (Sigma, 223530), 50 mM sodium bicarbonate (Sigma, 26014), 150 mM sodium chloride (Sigma, S3014) and 25 µM ethylenediaminetetraacetic acid (EDTA; Sigma, E5134), pH 10) for 24 h at 37 °C with gentle shaking. Samples were washed in carbonate buffer with 5 mM EDTA three times for 2 h at 37 °C with gentle shaking. Samples were incubated in blocking buffer overnight at 37 °C while shaking before incubating in primary antibodies to neurofilament (1:40 3A10 in blocking buffer) for 4 days at 37 °C while shaking. Embryos were washed six times (3 h each) in 0.1% Triton X-100 in 1 × PBS before staining with secondary antibodies (Biotium CF633 goat anti-mouse IgG, 20121, lot 23C1003; 1:300) and counterstained with DAPI (1:100) in blocking buffer for 4 days at 37 °C while shaking. Samples were then washed in 1 × PBS three times for 2 h each and postfixed overnight in 1 w/v% PFA in 1 × PBS overnight at 4 °C while shaking. Samples were washed with 1 × PBS for 2 h before preparing them for confocal microscopy.

Confocal imaging

Before imaging, the samples were placed in a refractive-index matching solution (45 w/v% antipyrine (Thermo Scientific, A11089.22), 30 w/v% nicotinamide (Thermo Scientific, A128271000) and 0.5 v/v% *N*-butyldiethanolamine in distilled water (CUBIC-R[70])) for 1–3 days (depending on the size of the embryonic sample), to render the tissues optically transparent for three-dimensional imaging. Samples were mounted on a 35-mm glass-bottom microscopy dish suspended in a solution of 0.5% low-melting-point agarose (Thermo Scientific, R0801) in CUBIC-R to avoid movement of the sample during the imaging process. The mounted samples were then covered with a glass coverslip. Samples were imaged with a Zeiss confocal laser scanning microscope (LSM 900) equipped with a Plan-Apochromat 25×/0.8 glycerol immersion objective and using a pinhole of 1 AU. Three-dimensional, whole-tissue volumes were acquired using a combination of *Z*-stacks and image tiling. Images were processed with Zen (Zeiss) and FIJI[74], and VGStudio Max 3.3 was used for three-dimensional visualization of the scans.

Reporting summary

Further information on research design is available in the Nature Portfolio Reporting Summary linked to this article.

Data availability

All original data are available via MorphoSource, including micro-computed tomography, synchrotron and confocal scans. Data are publicly available, except in cases in which the museum holds the copyright, for which data are available upon reasonable request via https://www.morphosource.org/projects/000626244.

Code availability

For synchrotron reconstruction, we used GSECARS Tomography Software, which is free to download via https://cars-uchicago.github.io/IDL_Tomography/index.html.

61. Miller, J., Loch, J. & Taylor, J. Biostratigraphy of Cambrian and Lower Ordovician strata in the Llano uplift, central Texas. Ch. 4. AAPG Mem. 98, 187–202 (2012).
62. Fortey, R., Landing, E. & Skevington, D. Cambrian-Ordovician boundary sections in the Cow Head Group, western Newfoundland. *Natl Mus. Wales Geol. Ser.* **3**, 95–129 (1982).

63. Raasch, G. O. *Cambrian Merostomata* (Geological Society of America, 1939).
64. Houée, G., Bardin, J., Germain, D., Janvier, P. & Goudemand, N. Developmental models shed light on the earliest dental tissues, using *Astraspis* as an example. *Palaeontology* **66**, e12682 (2023).
65. Smith, M. M. & Sansom, I. J. in *Development, Function and Evolution of Teeth* (eds. Teaford, M. F. et al.) 65–81 (Cambridge Univ. Press, 2000).
66. Mori, S. & Nakamura, T. Redeployment of odontode gene regulatory network underlies dermal denticle formation and evolution in suckermouth armored catfish. *Sci. Rep.* **12**, 6172 (2022).
67. Rivers, M. GSECARS Tomography Software — IDL Tomography Processing. *Github* https://cars-uchicago.github.io/IDL_Tomography/ (2023).
68. Onimaru, K., Motone, F., Kiyatake, I., Nishida, K. & Kuraku, S. A staging table for the embryonic development of the brownbanded bamboo shark (*Chiloscyllium punctatum*). *Dev. Dyn.* **247**, 712–723 (2018).
69. Gillis, J. A. et al. Big insight from the little skate: *Leucoraja erinacea* as a developmental model system. *Curr. Top. Dev. Biol.* **147**, 595–630 (2022).
70. Susaki, E. A. et al. Versatile whole-organ/body staining and imaging based on electrolyte-gel properties of biological tissues. *Nat. Commun.* **11**, 1982 (2020).
71. Chung, K. et al. Structural and molecular interrogation of intact biological systems. *Nature* **497**, 332–337 (2013).
72. Smith-Paredes, D. et al. Embryonic muscle splitting patterns reveal homologies of amniote forelimb muscles. *Nat. Ecol. Evol.* **6**, 604–613 (2022).
73. Griffin, C. T. et al. The developing bird pelvis passes through ancestral dinosaurian conditions. *Nature* **608**, 346–352 (2022).
74. Schindelin, J. et al. Fiji: an open-source platform for biological-image analysis. *Nat. Methods* **9**, 676–682 (2012).

Acknowledgements We thank the Shubin Lab members S. Ali, E. Hillan, D. Jockel and S. Kult Perry for early discussion and support; J. Miller for segmentation assistance and animal care; I. Sansom, S. Giels, J. Repetski, M. Webster, S. Bensmaia, N. Hughes, M. Coates, M. Friedman, A. R. C. Millner, M. Bonilla, T. Stewart and B. Engh for assistance, discussions and thoughtful comments; J. A. Maisano, D. Edey, M. W. Colbert and all of the University of Texas Computed Tomography Facility for initial scans; K. Duncan, G. Olack and A. Neander for assistance with additional scanning of specimens; P. Coorough Burke, W. Simpson, C. A. Eaton, M. Coyne, M. Flourence and C. Labanderia for providing access to fossil specimens; R. Bieler, J. Voight, K. Griffin-Jakym and M. Pryzdia for specimen access; C. Ferret for donating invertebrates from his personal collection and J. Garcia for *Ancistrus* specimens and catfish knowledge; A. Boersma for work on Fig. 5; and M. Yakovlev for assistance with synchrotron scanning. Portions of this work were performed at GeoSoilEnviroCARS (The University of Chicago, Sector 13), Advanced Photon Source, Argonne National Laboratory. GeoSoilEnviroCARS was supported by the National Science Foundation – Earth Sciences (EAR – 1634415). Tomography capability developments were supported by the Department of Energy Office of Basic Sciences Geosciences Research Program (DE-SC0020112). This research used resources of the Advanced Photon Source, a US DOE Office of Science User Facility operated for the DOE Office of Science by Argonne National Laboratory under contract number DE-AC02-06CH11357. Additional support was provided by the Brinson Family Foundation and the Biological Sciences Division of the University of Chicago.

Author contributions Y. H. and N.H.S. conceived and designed the project. K.N. and J.O.-H. provided direction and context for the invertebrate data collection and analysis. Fossil sample acquisition was carried out by Y.H., N.S., K.N., N.H.S., J.F.M. and J.O.-H. Fossil sample preparation was carried out by Y.H. and N.S. Synchrotron data collection was performed by Y.H., S.C.P.N., M.F., N.S., M.R., P.L.R. and N.H.S. Synchrotron data analysis was carried out by Y.H., S.C.P.N., N.S. and P.V. Sample preparation, immunostaining and imaging of *Ancistrus*, *Scyliorhinus* and *Leucoraja* was carried out by Y.H., S.C.P.N., M.F. and N.S. All segmented images, visualizations and figures (except Fig. 5) were prepared by Y.H. with input from all authors. The original draft was written by Y.H. and N.H.S. Review and editing of the manuscript was performed by Y.H., S.C.P.N., M.F., K.N., N.S., J.F.M., M.R., P.L.R., J.O.-H. and N.H.S.

Competing interests The authors declare no competing interests.

Additional information

Supplementary information The online version contains supplementary material available at https://doi.org/10.1038/s41586-025-08944-w.

Correspondence and requests for materials should be addressed to Yara Haridy or Neil H. Shubin.

Peer review information *Nature* thanks Philippe Janvier and the other, anonymous, reviewer(s) for their contribution to the peer review of this work. Peer reviewer reports are available.

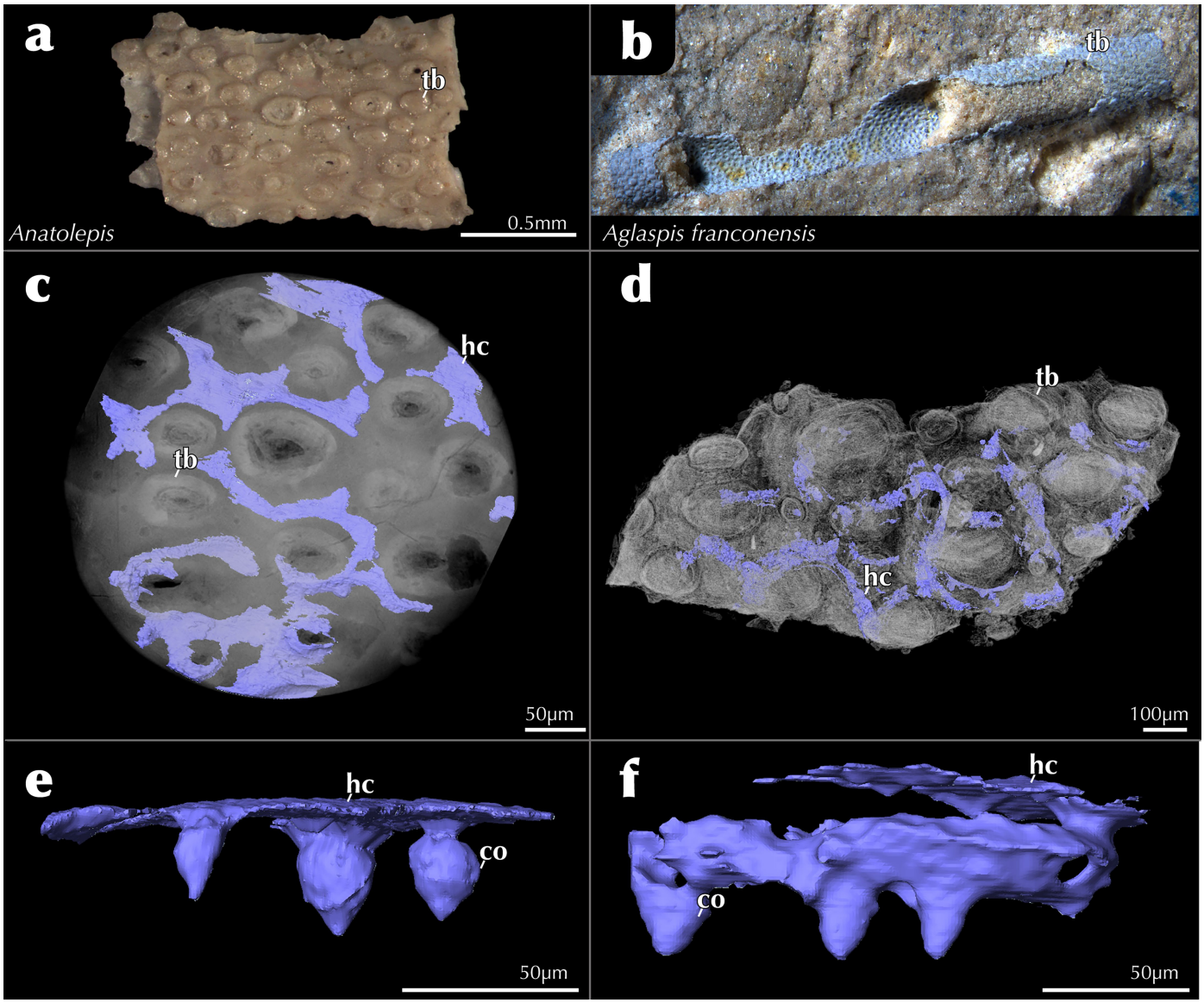

Extended Data Fig. 1 | Horizontal and vertical pore canal system in the *Anatolepis* fragments and the aglaspidid arthropod *Aglaspis? franconensis*. **a**, The late Cambrian *Anatolepis* sp. fragment from central Texas Wilberns Formation (TC-1021) from which a fragment was removed for scanning. **b**, The holotype of *Aglaspis? franconensis* USNM PAL 98916 from the late Cambrian St. Lawrence Formation of Wisconsin. **c**, Dorsal view of a translucent three-dimensional reconstruction of *Anatolepis* fragment with a distribution of horizontal canals that surround the tubricles. **d**, Dorsal view of a translucent three-dimensional reconstruction of *Aglaspis? franconensis* fragment with a distribution of horizontal canals that surround the tubercles. **e,f**, Segmented horizontal canals showing how they sometimes are attached to the cuticular organs, in *Anatolepis* and *Aglaspis? franconensis* respectively. Abbreviations: co, cuticular organ; hc, horizontal canal; tb, tubercle.

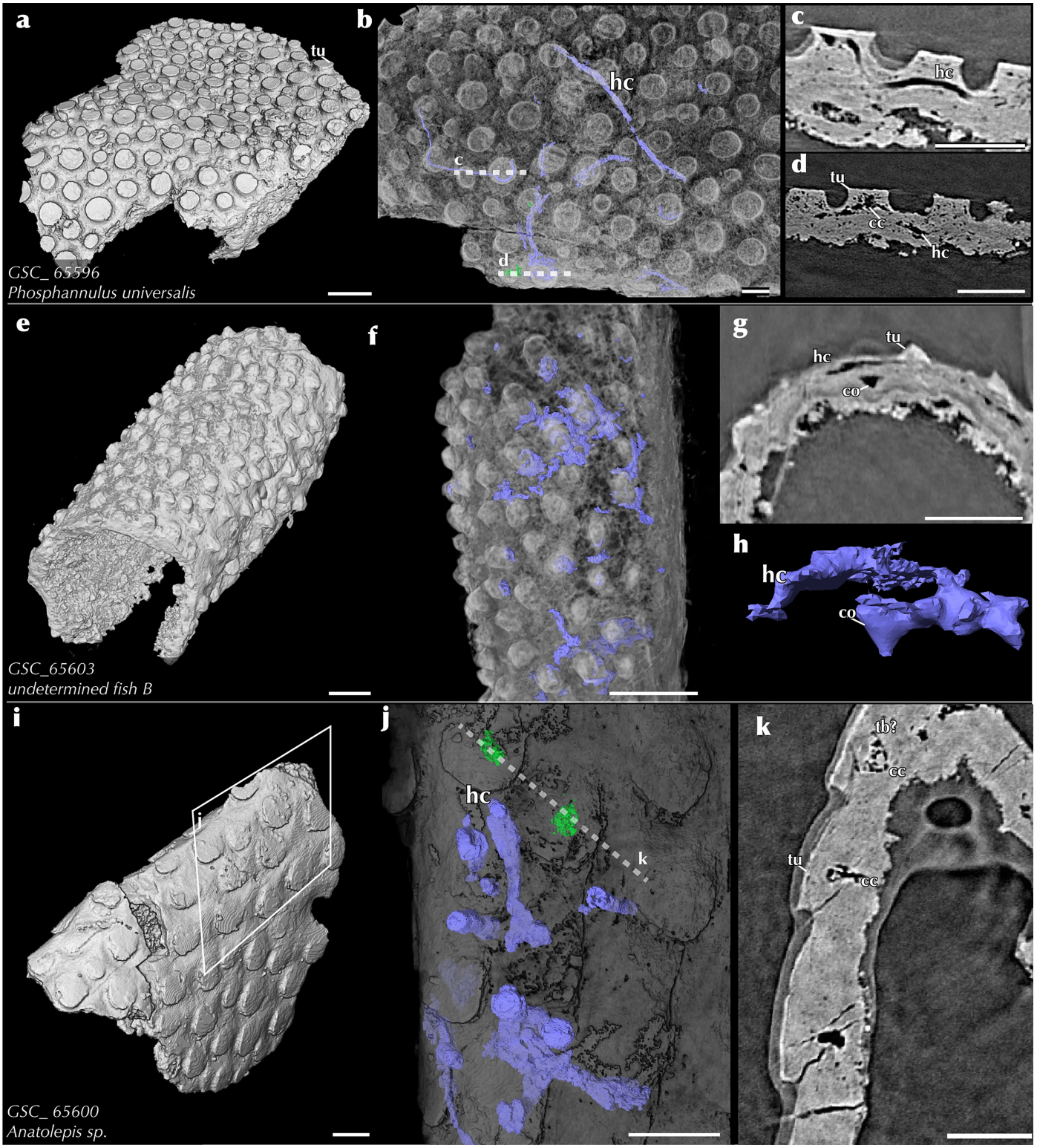

Extended Data Fig. 2 | Microstructure of the putative vertebrate fragments from the Cambrian-Ordovician Cow Head Formation in Newfoundland. **a**, A three-dimensional rendering of a specimen of *Phosphannulus universalis* (GCS65596) from the Cow Head formation. **b**, Magnification of the rendering of flat top tubercles, in purple are the segmented horizontal canals. **c,d**, Tomographic cross sections of cuticle showing that the horizontal canals run through the tubercles, unlike arthropods, but some tubercles have a central cavity similar to aglaspidid specimens. **e**, Three-dimensional rendering of a specimen of 'undetermined fish B' (GCS65603) from Cow Head Formation. **f**, Magnification of the rendering of the pointed tubercles, in purple are the segmented horizontal canals. **g**, Tomographic cross sections of cuticle showing presence of horizontal canals and a cuticular organ similar to aglaspidid arthropods. **h**, Rendering of a segmented horizontal canal and attached cuticular organ similar to previously figured known aglaspidid cuticle. **i**, Three-dimensional rendering of a specimen of '*Anatolepis*' (GCS65600) from Cow Head formation. **j**, Magnification of the rendering of the flattened pointed tubercles, in purple are the segmented horizontal canals. **k**, Tomographic cross sections of cuticle showing presence of central cavity in the tubercles, and possible tubules in tubercles, similar to other figured aglaspidids. Abbreviations: cc, central canal; co, cuticle organ; hc horizontal canal; tb?, possible tubule; tu, tubercle.

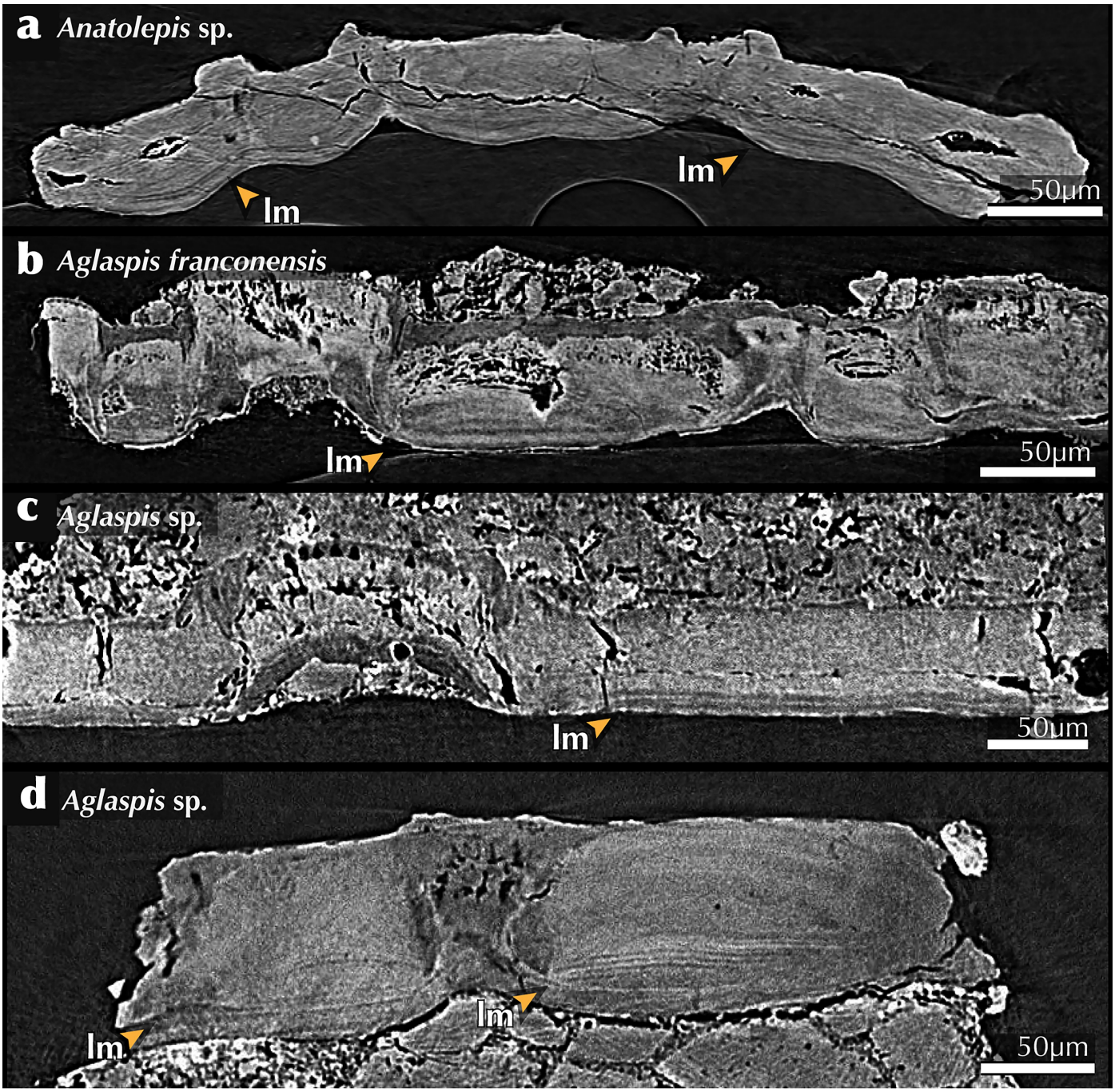

Extended Data Fig. 3 | Laminar cuticle structure of *'Anatolepis'* and aglaspidids arthropods. a, Tomographic cross section of *Anatolepis* cuticle showing the multiple layers at the base. **b** Tomographic cross section of *Aglaspis? franconensis* cuticle showing the multiple layers **c**, Tomographic cross section of *Aglaspis* sp. cuticle showing the multiple layers at the base, this specimen was taken from a body segment **d**, Tomographic cross section of *Aglaspis* sp. cuticle showing the multiple layers at the base, this specimen was taken from a tailspine segment. Abbreviations: lm, lamellae.

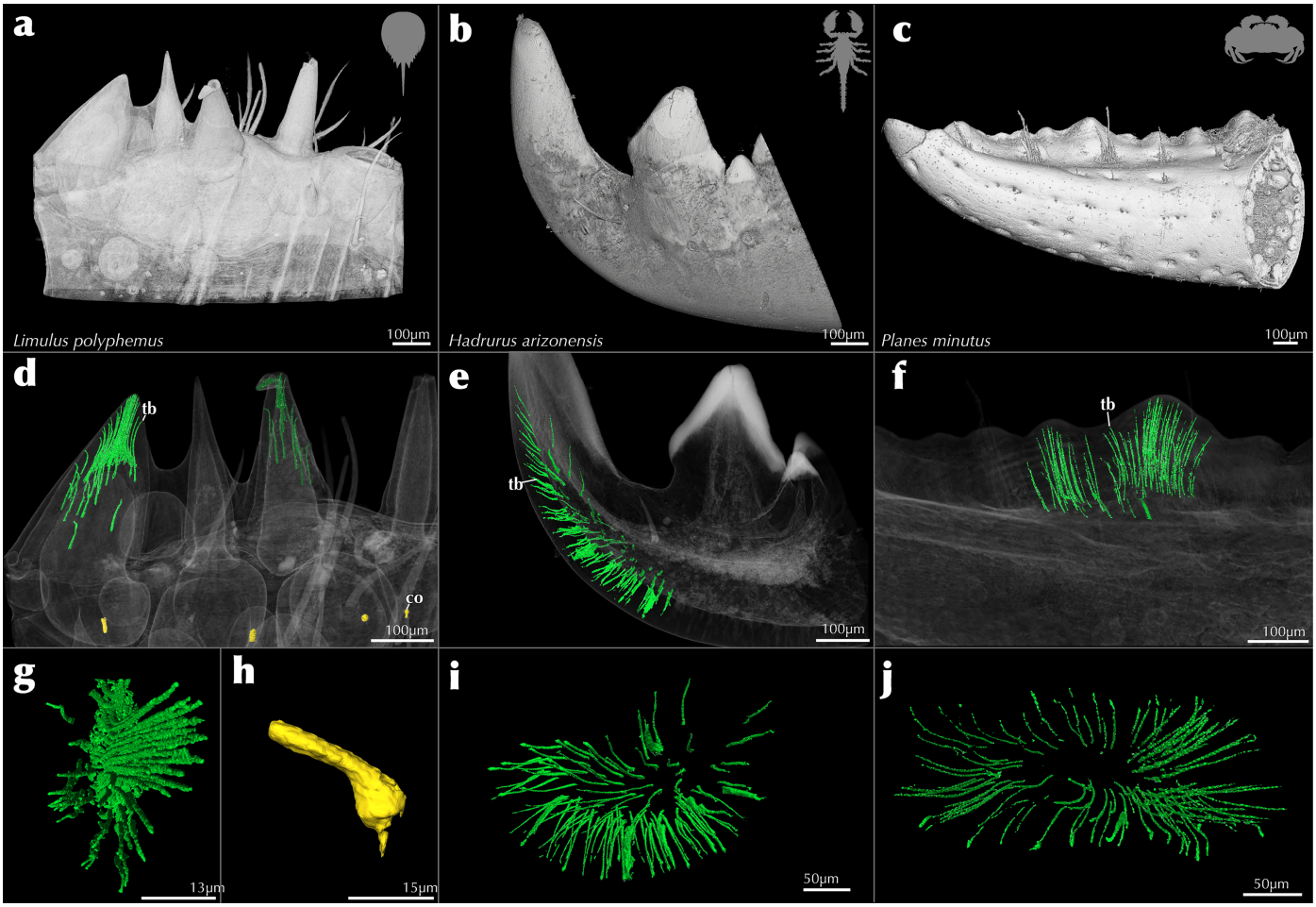

Extended Data Fig. 4 | Additional arthropod uCT data showing tubules within various cuticular elements. a-c, Atlantic horseshoe crab (*Limulus polyphemus*) gnathobase; Giant hairy scorpion (*Hadrurus arizonensis*) chelicerae; Columbus crab (*Planes minutus*) claw dactyl. **d-f**, Partially translucent renderings showing the prevalence of tubules in the cuticles of the aforementioned arthropods. **g,i,j**, Variation in tubule orientation when viewed dorsally. **h**, A cuticle organ like structure seen in the gnathobase of *Limulus*. Abbreviations: tb, tubule; co, cuticular organ.

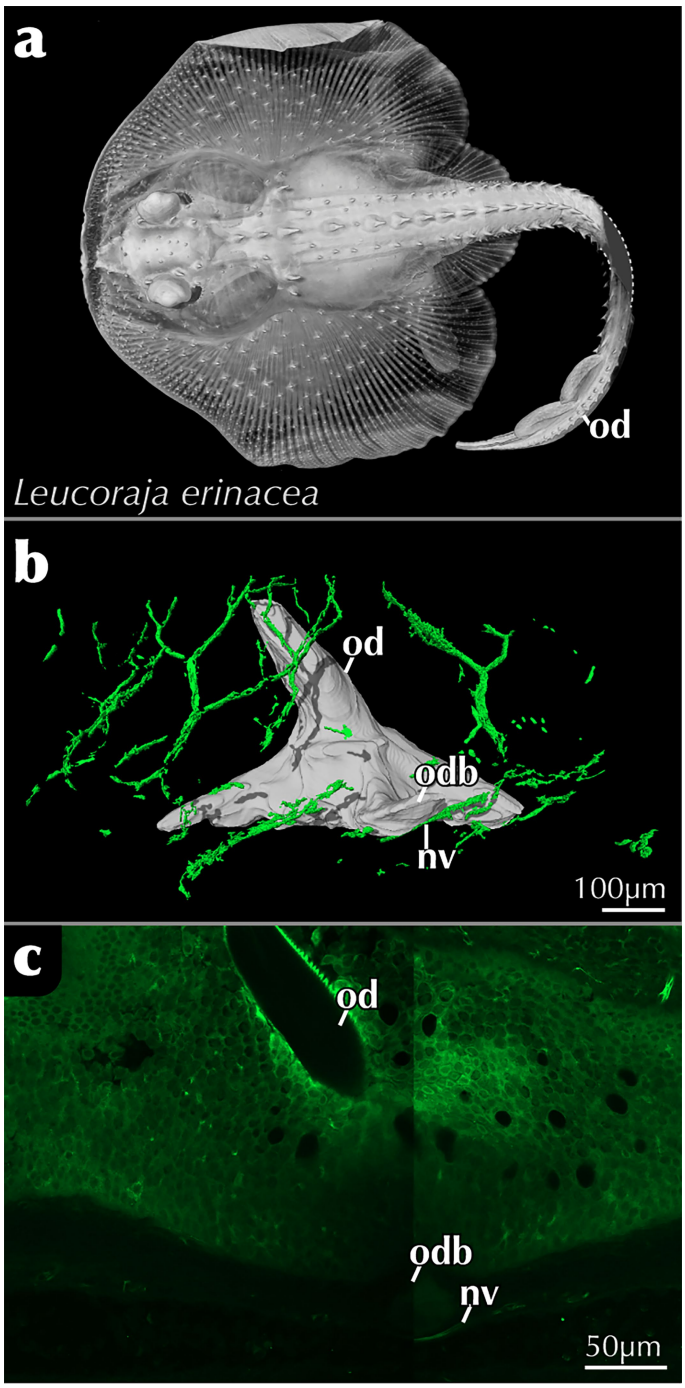

Extended Data Fig. 5 | Innervation of external odontodes in the little skate *Leucoraja erinacea*. **a**, µCT rendering of a stage 33 little skate (*Leucoraja erinacea*) showing the distribution of odontodes across the body, the odontodes samples for clearing and immunofluorescence were the distal most tail odontodes. **b**, Immunofluorescence confocal stack-based segmentation of tail odontodes with nerves branching and surrounding the odontode, note that the nerve is at the base of the odontode where foramina are observed in older specimens. **c**, Immunostained cross section of little skate single tail odontode, showing the innervation of the base of the odontode, the epidermis of the little skate is bright either due to autofluorescence or nonspecific antibody binding. This experiment was performed on one representative sample of the correct stage, n = 1. Abbreviations: od, odontode; odb, odontode base; nv, nerves.

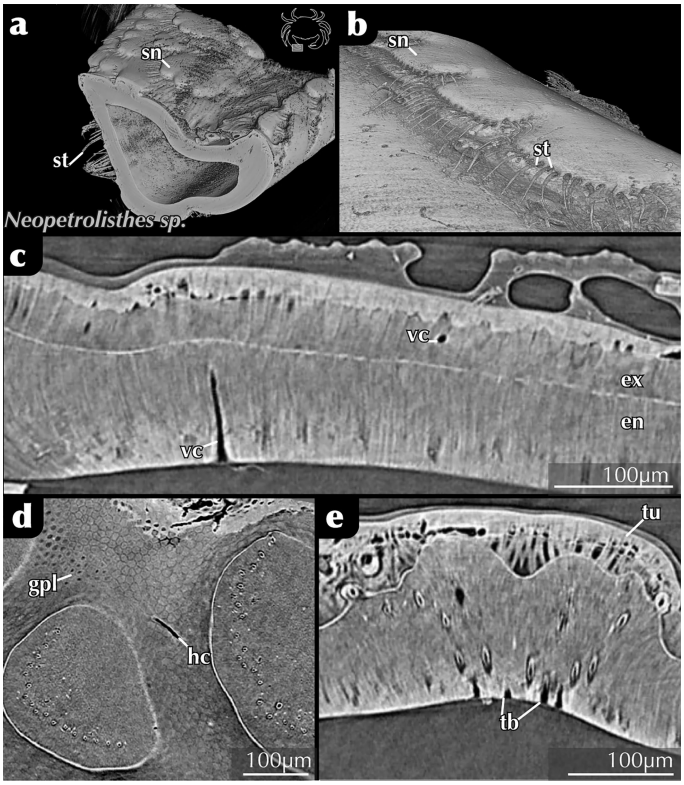

Extended Data Fig. 6 | Histology details of anomuran *Neopetrolisthes* sp. dactyl showing multilayered cuticle. a,b, Three-dimensional renderings of a portion of *Neopetrolisthes* sp. dactyl, showing the distribution of external sensilla with seta. **c**, Tomographic cross section of the cuticle showing the multiple layers and penetration of vertical canals. **d**, Tomographic dorsal cross section showing the distinctive granular polygonal layer described in (Young et al.[54]). **e**, Tomographic cross section of a single sensillum with vertical pores akin to those described in (Young et al.[54]). Abbreviations: ex, exocuticle; en, endocuticle; gpl, granular polygonal layer; hc horizontal canal; sn, sensillum; st, seta; vc, vertical canal.

Extended Data Table 1 | Scanned exoskeleton samples of diverse extant and extinct vertebrate and invertebrate specimens, highlighted samples are directly included in this study, while all others were examined but not segmented

#	Taxon	Origin	Sampled part	Scan type
1	*Limulus polyphemus* (Atlantic horseshoe crab)	Purchased online	Gnathobases and cuticle	Synchrotron µCT
2	*Hadrurus arizonensis* (Hairy desert scorpion)	Teaching collection	Chelicerae leg cuticle	Synchrotron µCT
3	*Callinectes sapidus* (Atlantic Blue Crab)	Purchased locally	Dactyl	Synchrotron µCT
4	*Petrolisthe galathinus* (Porcelain crab)	Donated by Charles Ferret	Dactyl and Leg cuticle	Synchrotron µCT
5	*Eupatorus gracilicornis* (five-horned rhinoceros beetle)	Purchased online	Leg cuticle and Wing shield	Synchrotron µCT
6	*Paracentrotus Lividus* (Purple Sea urchin)	FMNH 832	Spine	Synchrotron µCT
7	*Asterias Rubens* (common starfish)	FMNH 514	Spine	Synchrotron µCT
8	*Atya Crassa* (Freshwater shrimp)	FMNH 2891	Eye and Leg cuticle	Synchrotron µCT
9	*Megabalanus tintinnabulum* (Giant purple barnacle)	Purchased online	Shell Exoskeleton	Synchrotron µCT
10	*Goniopsis* sp. (mangrove crab)	FMNH 1674	Dactyl	Synchrotron µCT
11	*Panopeus* sp. (mud crab)	FMNH 2130	Dactyl	Synchrotron µCT
12	*Cardina* sp. (freshwater atyid shrimp)	FMNH 1307	Eye, Leg and thorax cuticle	Synchrotron µCT
13	*Glycymeris* sp. (bittersweet clam)	FMNH 346173	Shell	Synchrotron µCT
14	*Planorbarius corneus* (ramshorn snail)	Local aquarium store	Shell	Synchrotron µCT
15	*Anadra* sp. (saltwater bivalve)	FMNH 155152	Shell	Synchrotron µCT
16	*Meretrix* sp. (saltwater clam)	FMNH 184516	Shell	Synchrotron µCT
17	*Polites* sp. (North American grass skipping butterfly)	Donated by Charles Ferret	Antennae and Leg cuticle	Synchrotron µCT
19	*Planes miutus* (Columbus crab)	FMNH 12075	Dactyl	Synchrotron µCT
20	*Aglaspis spinifer*	MPM 11292	Phosphatic preserved cuticle	Synchrotron µCT
21	Aglaspidid	MPM 1857	Phosphatic preserved cuticle	Synchrotron µCT
22	*Aglaspis franconensis*	USNM- PAL 98196	Phosphatic preserved cuticle	Synchrotron µCT
23	*Euriptrid* sp.	UWGM 2346	Preserved cuticle	Synchrotron µCT
24	Elrathia Trilobite	UWGM 1106.1	Calcite cuticle	Synchrotron µCT
25	Brachiopod	MPM 7121	Preserved shell with matrix	Synchrotron µCT
26	*Anatolepis* sp.	FMNH TC-1021	Phosphatic preserved cuticle	Synchrotron µCT
27	*Cyclopina Vulgaris*	MPM 11927	Phosphatic preserved cuticle	Synchrotron µCT
28	*Astraspis* sp.	FMNH PF 17898	Isolated odontodes on bone	Synchrotron µCT
29	*Eriptychius* sp.	FMNH PF17901	Isolated odontodes on bone	Synchrotron µCT
30	*Pterygolepis nitidus*	ROM VP 49213	Headshield	Synchrotron µCT
31	*Trematapsis mammillata*	MFN	Headshield	Synchrotron µCT
32	Unknown Conodont	UWGM 738	Isolated pharyngeal elements	Synchrotron µCT
33	*Ancistrus* sp.	Reared at University of Chicago	Tail, pectoral fin and body odontodes	Synchrotron µCT; Confocal; µCT whole
34	*Scyliorhinus retifer*	MBL	Distal tail odontodes	Confocal image stack; µCT whole
35	*Leucoraja erinacea*	MBL	Distal tail odontodes	Confocal image stack; µCT whole

nature portfolio

Corresponding author(s): Yara Haridy

Last updated by author(s): 2025/01/27

Reporting Summary

Nature Portfolio wishes to improve the reproducibility of the work that we publish. This form provides structure for consistency and transparency in reporting. For further information on Nature Portfolio policies, see our Editorial Policies and the Editorial Policy Checklist.

Statistics

For all statistical analyses, confirm that the following items are present in the figure legend, table legend, main text, or Methods section.

n/a	Confirmed
☐	☒ The exact sample size (*n*) for each experimental group/condition, given as a discrete number and unit of measurement
☐	☒ A statement on whether measurements were taken from distinct samples or whether the same sample was measured repeatedly
☒	☐ The statistical test(s) used AND whether they are one- or two-sided *Only common tests should be described solely by name; describe more complex techniques in the Methods section.*
☒	☐ A description of all covariates tested
☒	☐ A description of any assumptions or corrections, such as tests of normality and adjustment for multiple comparisons
☒	☐ A full description of the statistical parameters including central tendency (e.g. means) or other basic estimates (e.g. regression coefficient) AND variation (e.g. standard deviation) or associated estimates of uncertainty (e.g. confidence intervals)
☒	☐ For null hypothesis testing, the test statistic (e.g. *F*, *t*, *r*) with confidence intervals, effect sizes, degrees of freedom and *P* value noted *Give P values as exact values whenever suitable.*
☒	☐ For Bayesian analysis, information on the choice of priors and Markov chain Monte Carlo settings
☒	☐ For hierarchical and complex designs, identification of the appropriate level for tests and full reporting of outcomes
☒	☐ Estimates of effect sizes (e.g. Cohen's *d*, Pearson's *r*), indicating how they were calculated

Our web collection on statistics for biologists contains articles on many of the points above.

Software and code

Policy information about availability of computer code

Data collection

Acquisition of the µCT data set
Synchrotron micro computed tomography was performed at beamline 13-BM-D at the Advanced Photon Source at Argonne National Laboratory. The white X-ray beam from the APS bending magnet was reflected from a Pt-coated mirror at 3 mrad incidence angle, producing an energy spectrum centered at ~25 keV with ~10 keV bandwidth. 3600 projection views were acquired over 180 degrees using a Point Grey Grasshopper 3 camera, with 1920 (H) X 1200 (V) pixels, viewing a LuAG scintillator. The sample-to-scintillator distance was approximately 45 mm. Depending on the sample, the camera was equipped with either a 10X or 5X Mitutoyo long-working distance objective lens. For both objectives, a 175 mm tube was used, resulting in 0.56-micron pixels in object space for the 10X lens and 1.09 micron pixels in object space for the 5X lens. The exposure time was 0.014 seconds per view for the 10X lens and 0.025 seconds per view for the 5X.

The reconstruction software is hosted here:https://github.com/CARS-UChicago/IDL_Tomography This shows the version information (tags).https://github.com/CARS-UChicago/IDL_Tomography/tags. Versions R0, R1, and R2 were used.

Laboratory micro computed tomography was performed on a Phoenix v|tome|x S 240 from GE (PaleoCT facility, RRID:SCR024763, University of Chicago)

Data analysis

Synchrotron micro computed tomography images were reconstructed using the GSECARS tomography processing software (https://cars-uchicago.github.io/IDL_Tomography/)14, which dark-current corrects and white-field normalizes the acquired data prior to performing gridding-based image reconstruction. The resulting image voxel sizes are 0.56x0.56x0.56 microns for the 10X configuration and 1.09x1.09x1.09 microns for the 5X configuration. Experiment run at GSECARS; Proposal GUP: 82458; Proposal Title: "Characterizing the origin

and development of the earliest mineralizing tissues in vertebrates using synchrotron microCT"; Experiment Date: 2023-03-21 and 2022-12-02.
Segmentation, reconstruction, and visualization were performed on Amira 3D 2021.1 (©1995-2001 Konrad-Zuse-Zentrum Berlin (ZIB), ©1999-2021 FEI SAS, a part of Thermo Fisher Scientific).

Confocal imaging
Three dimensional, whole-tissue volumes were acquired using a combination of Z-stacks and image tiling. Images were processed with Zen (Zeiss) and FIJI21 and VGStudio Max 3.3 was used for three-dimensional visualization of the scans.

For manuscripts utilizing custom algorithms or software that are central to the research but not yet described in published literature, software must be made available to editors and reviewers. We strongly encourage code deposition in a community repository (e.g. GitHub). See the Nature Portfolio guidelines for submitting code & software for further information.

Data

Policy information about availability of data

All manuscripts must include a data availability statement. This statement should provide the following information, where applicable:

- Accession codes, unique identifiers, or web links for publicly available datasets
- A description of any restrictions on data availability
- For clinical datasets or third party data, please ensure that the statement adheres to our policy

Data Availability:
All original data is on Morphosource, including µCT, Synchrotron and Confocal scans. Data is be publicly available, except where the museum holds the copyright then data are available upon reasonable request: https://www.morphosource.org/projects/000626244

Research involving human participants, their data, or biological material

Policy information about studies with human participants or human data. See also policy information about sex, gender (identity/presentation), and sexual orientation and race, ethnicity and racism.

Reporting on sex and gender	N/A
Reporting on race, ethnicity, or other socially relevant groupings	N/A
Population characteristics	N/A
Recruitment	N/A
Ethics oversight	N/A

Note that full information on the approval of the study protocol must also be provided in the manuscript.

Field-specific reporting

Please select the one below that is the best fit for your research. If you are not sure, read the appropriate sections before making your selection.

☐ Life sciences ☐ Behavioural & social sciences ☒ Ecological, evolutionary & environmental sciences

For a reference copy of the document with all sections, see nature.com/documents/nr-reporting-summary-flat.pdf

Ecological, evolutionary & environmental sciences study design

All studies must disclose on these points even when the disclosure is negative.

Study description	This study's aim is to qualatativly describe the micro-structure of vertebrate odontodes and invertebrate cuticular structures. No quantitative analysis was performed.
Research sample	The sample size of fossil material was dependent on availability and destructive sampling permissions. Extant taxa sampling was dependent on availability in museum collections and number of animals donated.
Sampling strategy	Sample size was limited to the fossil specimens of appropriate preservation and locality. Extant animal scans were limited to donated specimens or specimens available at museums often (n=1)
Data collection	All Synchrotron data, and µCT data was collected by the first author. Confocal data was collected by the second author.

Timing and spatial scale	Data was collected when synchrotron beam time and µCT scantime was allocated.
Data exclusions	No data was excluded.
Reproducibility	µCT scans were not subject to reproducibility. Antibody staining was conducted on several specimens not included in this study to verify findings.
Randomization	Randomization was not possible as the limited specimens were selected, scanned,and segmented by the first author.
Blinding	Blinding was not possible as the limited specimens were selected, scanned,and segmented by the first author.

Did the study involve field work? ☐ Yes ☒ No

Reporting for specific materials, systems and methods

We require information from authors about some types of materials, experimental systems and methods used in many studies. Here, indicate whether each material, system or method listed is relevant to your study. If you are not sure if a list item applies to your research, read the appropriate section before selecting a response.

Materials & experimental systems

n/a	Involved in the study
☐	☒ Antibodies
☒	☐ Eukaryotic cell lines
☐	☒ Palaeontology and archaeology
☐	☒ Animals and other organisms
☒	☐ Clinical data
☒	☐ Dual use research of concern
☒	☐ Plants

Methods

n/a	Involved in the study
☒	☐ ChIP-seq
☒	☐ Flow cytometry
☒	☐ MRI-based neuroimaging

Antibodies

Antibodies used	(Cy3 donkey anti-mouse IgG, Jackson laboratories, 715-165-150, LOT: 163873; 1:300) // Antibody 3A10 (Registry ID: AB_531874) was used; company: DSHB https://dshb.biology.uiowa.edu/3A10//4′,6-Diamidino-2-Phenylindole, dihydrochloride (DAPI) (Biotium, 40009, Lot: 15D1117;1:1000)
Validation	Validation from the manufacturer: “Confirmed Species Reactivity: Chicken, Fish, Gecko, Human, Mouse, Planaria, Quail, Rat, Shark, Xenopus, Zebrafish” Validation on Catfish was performed by: Catfish validation: Hardy et al. 2016 DOI: 10.1098/rspb.2015.2652

Palaeontology and Archaeology

Specimen provenance	No new material was collected for this study.
Specimen deposition	Specimens figured in this study are deposited at the following institutions: MPM- Milwaukee Public Museum UWGM- University of Wisconsin Geology Museum GSC- Geological survey of Canada USNM- Smithsonian National Museum of Natural History FMNH- Field Museum of Natural history MBL- Marine Biological laboratory
Dating methods	No new dates are provided

☐ Tick this box to confirm that the raw and calibrated dates are available in the paper or in Supplementary Information.

Ethics oversight	No new material was collected for this study. All use, destructive sampling and imaging permissions were provided by the following: Milwaukee Public Museum- Patricia Coorough Burke

University of Wisconsin Geology Museum- Carrie A. Eaton
Smithsonian National Museum of Natural History- Conrad Labandeira
Field Museum of Natural history- William Simpson

Note that full information on the approval of the study protocol must also be provided in the manuscript.

Animals and other research organisms

Policy information about studies involving animals; ARRIVE guidelines recommended for reporting animal research, and Sex and Gender in Research

Laboratory animals	Ancistrus sp. (Bristle nose catfish)- 3 weeks Leucoraja erinacea (little skate)- stage 31-33 Scyliorhinus retifer (cat sharks)- stage 38 All invertebrates were from the Field Museum of Natural History, or donated as specimens. Limulus polyphemus (Atlantic horseshoe crab) Hadrurus arizonensis (Hairy desert scorpion) Callinectes sapidus (Atlantic Blue Crab) Petrolisthe galathinus (Porcelain crab) Eupatorus gracilicornis (five-horned rhinoceros beetle) Paracentrotus Lividus (Purple Sea urchin) Asterias Rubens (common starfish) Atya Crassa (Freshwater shrimp) Megabalanus tintinnabulum (Giant purple barnacle) Goniopsis sp. (mangrove crab) Panopeus sp. (mud crab) Cardina sp. (freshwater atyid shrimp) Glycymeris sp. (bittersweet clam) Anadra sp. (saltwater bivalve Planorbarius corneus (ramshorn snail) Anadra sp. (saltwater bivalve) Meretrix sp. (saltwater clam) Polites sp. (North American grass skipping butterfly) Planes miutus (Columbus crab)
Wild animals	The study did not involve wild animals
Reporting on sex	This information was not collected.
Field-collected samples	The study did not involve field collected samples
Ethics oversight	The Institutional Animal Care and Use Committees of the University of Chicago approved the care and breeding of Ancistrus sp. (Bristle nose catfish) (IACUC# 72734). All the procedures were performed at the University of Chicago. The hatchling Leucoraja erinacea (little skate) and hatchling Scyliorhinus retifer (cat sharks) were obtained from the Marine Resources Center, Marine Biological Laboratory, Woods Hole, MA, USA.

Note that full information on the approval of the study protocol must also be provided in the manuscript.

Plants

Seed stocks	N/A
Novel plant genotypes	N/A
Authentication	N/A